UNIVERSITÀ DEGLI STUDI DI PADOVA

Dipartimento di Fisica e Astronomia "Galileo Galilei"

Corso di Laurea Magistrale in Fisica

Tesi di Laurea

Matter-wave interferometry in the time-domain

Relatore

Prof. Cinzia Sada

Correatore

Prof. Markus Ardnt

PhD Armin Shayeghi

Laureando

Andrea Grimaldi

Anno Accademico 2017/2018

ABSTRACT

In this thesis we present the last results obtained by OTIMA, one of the experiments of the Quantum Nanophysics group in Vienna and its name is an acronyms for **O**ptical **TI**me-domain **MA**tter-wave interferometer. In particular we will propose and discuss a new method to estimate the Visibility and we will show the last interfere measurement with $AgSF_2$, tailored nanoparticles that were specially designed to achieve interference with high mass.

CONTENTS

INTRODUCTION

In this thesis we present the last results obtained by OTIMA, one of the experiments of the Quantum Nanophysics group in Vienna and its name is an acronyms for **O**ptical **TI**me-domain **MA**tter-wave interferometer.

This experiment has two main goal. The first one is to achieve interference using matter with high masses in order to experimentally verify Collapse Wave-function Models[1]. The other one, that will not be discuss in this thesis, is to exploit the high sensitivity of the matter-wave interferometer in order to assist spectroscopy measurements[2].

MAtter-wave interference is based directly on the de Broglie hypothesis: every particle can behave as a wave with wavelength proportional to its momentum. Starting from this idea and using adequate diffraction grating, it is possible to produce an interference pattern in which the detection probability of a particle is modulated. Since this phenomenon is only described by the quantum mechanics and there is not a classical equivalent, matter-wave interference is the most direct way to understand the quantum-to-classical transition and in particular at which scale it happens.

In particular OTIMA is a **TI**me-domain interferometer that means, an interferometer that looks at the interference pattern formation in time and not in space. This peculiarity is both the most complicated and important aspect of this experiment. The general idea is that, due to the fact that momentum and wavelength of a particle are correlate, the interference fringes dynamically evolve allowing their study in function of time. This method gives the relevant advantage of marginalizing the velocity effect into the interference process and relaxes the beam preparation boundary.

The remain letter in the acronyms stands for **O**ptical and it refers to the gratings that are indeed made by light standing-waves. In fact in order to achieve a time-domain measure of the interference pattern it is necessary to have some kind of gratings that can appear and disappear in a very short time. The only possibility to achieve that is to mimic the interaction between a particle and a grating using the optical field generated by a standing wave.

As we said before one of the goal is to achieve interference with high mass particles and the first measurement of Otima has been done using the Even-Lavie valve[3]. This source is based on the supersonic expansions of a carrying gas that helps both the launch and the formation of

molecular clusters. Using the particle beam produced in this way, OTIMA showed interference with cluster of Anthracene(12th)[4], Vanillin(11th), Hexafluorobenzene(5th)[5] and Ferrocene(8th)[6], reaching its first mass record of 2139 u. After that the source was changed with a laser desorption one, in order to switch from supersonic velocity ($600\,m\,s^{-1} \sim 800\,m\,s^{-1}$) to thermal one ($300\,m\,s^{-1} \sim 400\,m\,s^{-1}$).

With this thermal beam OTIMA was able to achieve long Talbot Time configuration and measured interference with higher masses: TPP(614 u), $TPPF_{84}$(2815 u) and in particul $TPPF(20 - x + 17x)$ that upgraded the OTIMA mass record up to 5560 u [7]. In order to overcome the actual mass record for interference measurement that is still held by KDTL[8] we tried to use tailored nanoparticles. With this particles we achieved interference measurement with masses up to 1590 u,but had not overcome the OTIMA mass record.

In this thesis we will try to explain why these particles do not work out. In Chapter 1 we will introduce the theoretical framework that holds to model and understand the Physics behind OTIMA interferometer. In Chapter 2 we will present the experimental setup and in particular we discuss the data processing necessary to obtain a Visibility measurement. In the last part of this Thesis, Chapter 3, we will present the results of OTIMA within the tailored nanoparticles.

1

THEORY BEHIND THE OTIMA INTERFEROMETER

OTIMA is an Optical TIme-domain MAtter-wave interferometer. This acronyms summarizes everything of the experiment and every words has an important meaning that need an explanation.

INTERFEROMETER

MATTER WAVE

Mater waves are formulated by de Broglie hypothesis: all massive particles can exhibit wave-like properties with a wavelength determinated by their momentum, $\lambda = \frac{h}{p}$. This means that a particle can behave like a wave and, as a wave, can be diffracted, reflected or splitted by matter-wave "optics" devices. In particular, in 1991 diffraction of atoms was verified in [9], and starting form that decade the experimental technique has been exponentially improved to achieve interference with masses up to 10 123 u [8].

As explained in [10], the best framework to study the propagation and the manipulation of a matter wave is the Wigner representation. The basic idea of this formalism is to describe the system status in the phase-space through a real-value distribution $W(x,p)$. This distribution has to fulfill the axioms of *quasi-probability*, i.e.:

$$\int_{\mathbf{R}} dx\ W(x,p) = w(p),$$
$$\int_{\mathbf{R}} dp\ W(x,p) = w(x),$$
$$\int_{\mathbf{R}^2} dx\,dp\ W(x,p) = 1.$$

where $w(x)$ and $w(p)$ are the quasi-probability distribution of the position and momentum respectively.

The term *quasi* attribute to these distributions is due to their possibility of assuming negative value. This is a quantum properties that does does not have a classical equivalent and in particular negative value of the Wigner function identify the quantum nature of a process.

Those functions are connected to the density operators that live in the Hilbert space by:

$$W(x,p) = \frac{1}{2\pi\hbar}\int_{\mathbf{R}} ds e^{-i\frac{ps}{\hbar}} \langle x - \frac{s}{2}|\rho|x + \frac{s}{2}\rangle ,$$

that allow to translate the dynamic equation for the Wigner function into:

$$\left(\frac{\Delta}{\Delta t} + \frac{p}{m}\frac{\Delta}{\Delta x} - \frac{\Delta V(x;t)}{\Delta x}\frac{\Delta}{\Delta p}\right) W_t(x,p) = \sum_{l=1}^{\infty} \frac{(-)^l(\hbar/2)^{2l}}{(2l+1)!}\frac{\Delta^{2l+1}}{\Delta p^{2l_1}} W_t(x,p)$$

that is called *quantum Liouville equation*. The term on the right is the quantum correction to the classical equation but it does not simply distinguish the two behaviors. In fact this term is neglected in two different cases, the first one is the classical limit where $\hbar \to 0$, the other is when the $\Delta^{2l+1}V(x;t) \to zero$ for $l \geqslant 1$. This is very crucial when the quantum nature of a phenomena should be verified.

An other necessary ingredient to model a matter-wave interferometer is the *eikonal approximation*. This approximations is needed in order to reduce the complexity of the Liouville equation and can be fulfilled if the interaction time is enough short, namely if $\Delta t\sqrt{\frac{2|V|}{m}}$ is smaller that the characteristic length of the potential respectively. In this case the dynamic equation becomes:

$$\frac{\delta}{\delta t} W_t(x,p) = \sum_{l=0}^{\infty} \frac{(-)^l(\hbar/2)^{2l}}{(2l+1)!}\frac{\Delta^{2l+1}}{\Delta p^{2l_1}} W_t(x,p).$$

The big advantage of this approximation is that it allows to resolve the dynamics by means of the Fourier transforms and rewriting the evolution as a "step process":

$$W_{t_0+\Delta t}(x,p) = \int_{\mathbf{R}} dp_0 W_{t_0}(x,p_0) T_W(x,p-p_0). \tag{1.1}$$

In this way we can represent the evolution through, the convolution kernel $T_W(x,p_0)$, that in general is given by:

$$T_W(x,p_0) = \frac{1}{2\pi\hbar}\int_{\mathbf{R}} ds \exp\left[i\frac{p\,s}{\hbar} + i\,\varphi\left(x - \frac{s}{2}\right)) - i\,\varphi\left(x + \frac{s}{2}\right))\right]$$

(1.2)

where the potential is represented by the *eikonal phase* $\varphi(x)$ given by its time integration:

$$\varphi(x) = \int_{t_0}^{t_0+\Delta t} dt V(x;t).$$

In this way we just need to characterized the single interaction, as grating and free path, and combine them following the step-like evolution.

INTERFEROMETER

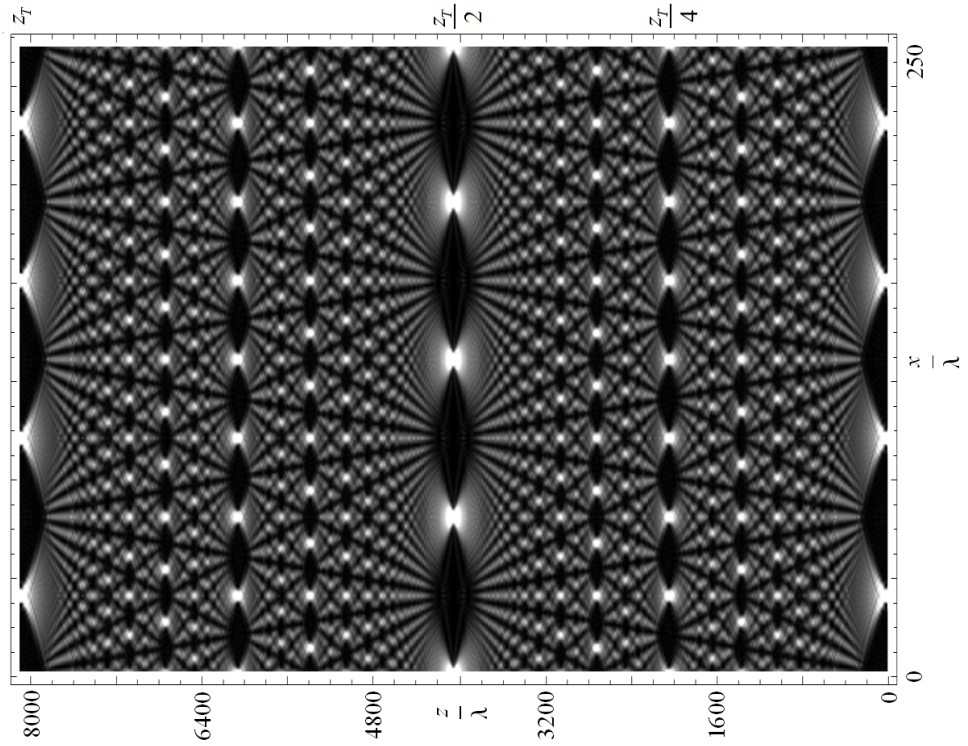

Figure 1.1: A simulation of the Talbot carpet. CC BY-SA 3.0, https://commons.wikimedia.org/w/index.php?curid=33862763

The physical principle on which OTIMA is based is the Talbot effect, an near-field diffraction phenomena. As in the case of optics, near-field refers to configurations where the waves will propagate for distance proportional to their wavelength and, in particular, the Talbot effect describes the interference pattern produced close to a *diffracting grating*.

In Figure 1.1 is reported the intensity modulation of a plane wave that passed through a grating with slits spacing d. As we can see the interference is a fractal pattern based on the grating geometry and distance T_L,

called Talbot length and defined by the wavelength and the slits spacing:

$$L_T = \frac{d^2}{\lambda} \tag{1.3}$$

The kernel of the fractal pattern is the grating image, that is periodical reproduced at distance $k\,L_T$, where $k \in \mathbb{Q}$ and it is called "order". This parameter collects all the information about the image reproduced by the interference pattern, in particular its shifting and scaling: when k is an integer the wave intensity reproduces the image of the grating with the same dimension and shifted by $n\,\frac{d}{2}$. On the other hand if $k = \frac{n}{q}$ with n and q coprime the image is scaled by a factor $\frac{1}{q}$ and shifted by $\frac{n}{q}\frac{d}{2}$.

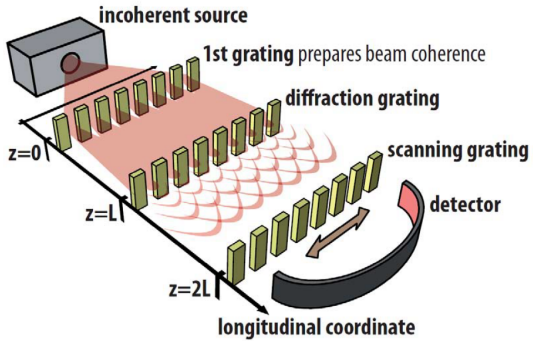

Figure 1.2: In this figure is reported the ideal scheme for a Talbot-Lau interferometer with three gratings. As we can see the incoherent beam is prepared by the *first grating*, diffracted by the *second grating* and scanned by the *third grating*.

The initial request for the Talbot effect is a plane wave that, in case of matter-wave, it is quite complicated to produce. In general the source has a finite size that can be approximated by a point like one from which a spherical wave is produced. This kind of wave can be reshaped to a usable approximation of a plane one but it can require collimation and a great distance between the source and the gratings, leading to a significant decrease of the signal intensity. In order to avoid this we can use the Talbot-Lau effect, that is an extension of what discussed before.

In case of a Talbot interferometer, we can relax this request of plane wave inasmuch the interference occurs if at least two neighboring apertures are coherently illuminated. A solution to fulfill this, is the Talbot-Lau effect, where an additional grating with the same slits separation is used to prepare the wave. This *preparation grating* will act an array of point like source and, if we put it at a Talbot length before the diffraction grating, the last one will be coherently illuminated.

An other problem is to resolve the interference pattern: due to the fact that it is an image of the grating, the fringes separation will be equal at

most to the slits separation and it will be independent of the beam wavelength. Instead of recording the intensity long on the traversal direction we can use an third grating with the same slits separation of the others as if it is an array of detectors. In order to do it, we need to put this *detection gratings* at a distance where we expect an imaging of the diffraction grating and record the signal in function the shift δx between their apertures. In this way the maximum signal will get when the $\delta x = nd$ and a minimum when $\delta x = n\frac{d}{2}$.

Interforemeter theory

In summary, OTIMA is based on a Talbot-Lau interferometer based on three gratings: the first one is used to prepare the coherence of the beam, the second one is responsible for the diffraction and the third one allows to discriminate the interference pattern produced. Based on this concepts, a model of matter-wave interferometer based on the Talbot-Lau effect was formulate by Nimmrichter and Hornberger [11].

Using the framework described in the Section 1.1.1, we can model the evolution of the particle beam as follows:

BEAM PREPARATION Here the beam is generated from the source and prepared in order to enter the interferometer: the sources initial distribution and the collimation, are represented by a first Wigner function $D(x, p)$. In particular here we assumed that the beam average trajectory is perfectly orthogonal to the gratings, so that $\langle p \rangle = 0$;

FIRST GRATING The particles beam interacts with the first grating and, using the Eq. 1.1 we can calculate $(W^{(1)}(x, p))$;

FREE PATH Now the beam modulated by the first grating freely travels to the second grating. It will travel a distance of L_1 in a time T_1. Beside the free evolution, given by $(W^{(1)}(x - \frac{p}{m}T_1, p))$, the particle can accumulate a shift both on position and momentum, so the Wigner function that reaches the second grating is given by $W^{(1)}(x - \frac{p}{m}T_1 + \delta x_1(T_1)), p + \delta p_1(T_1))$;

SECOND GRATING The coherent beam interacts with the second grating and it wave-function is diffracted, Again, we use the Eq. 1.1 to calculate $(W^{(2)}(x, p))$. Now the Wigner distribution represents the Talbot carpet generated.

FREE PATH The particles beam propagate freely until the last grating taking a Time T_2 to travel a distance L_2. Here too, the distribution can accumulate a shift both on position and momentum: $W^{(2)}(x - \frac{p}{m}T_2 + \delta x_2(T_2)), p + \delta p_2(T_2))$.

THIRD GRATING Here the beam is interacting with the last grating, that can be shifted of δx_s, and the Wigner function will became ($W_{t_3}(x,p)$). This one is finally integrate into the signal $S(\delta x_s)$;

Following these steps we express the signal $S(\delta x_s; L_1, L_2)$ expected after the interferometer as:

$$S(\delta x_s; L_1, L_2) = \int dx \sum_{l,k} \widetilde{D}\left(\frac{k L_1 + l L_2}{L_T} d\right) B_k^{(1)}\left(\frac{k L_1 + l L_2}{L_T}\right) B_{l-k}^{(2)}\left(l\frac{L_2}{L_T}\right) \exp\left[i\frac{2\pi}{d}(lx - l\delta x_2 + (l-k)\delta x_1)\right] \left|t^{(3)}(x-\delta x_s)\right|^2 \quad (1.4)$$

where $L_T = \frac{hd^2}{p_z}$ is the Talbot length, $\widetilde{D}$ is the Fourier transform of the initial transversal momentum distribution and $B_k^{(i)}(\xi)$ is the *Talbot coefficients* of the i-th grating. Theses terms are given as reformulation of the kernel functions in case the potential presents a periodicity. In particular we can rewrite a kernel function as:

$$T_W(x,p) = \frac{1}{2\pi\hbar}\sum_{n\in\mathbb{Z}} \exp\left[i\frac{2\pi x}{d}n\right]\int_{\mathbb{R}} ds\, e^{i\frac{sp}{\hbar}} B_n\left(\frac{s}{d}\right) \quad (1.5)$$

where the Fourier coefficients,

$$B_n(\xi) = \frac{1}{d}\int_{-\frac{d}{2}}^{+\frac{d}{2}} dx\ \exp\left[i\frac{2\pi x}{d}n + i\varphi\left(x - d\frac{\xi}{2}\right) - i\varphi\left(x + d\frac{\xi}{2}\right)\right] \quad (1.6)$$

are exactly the Talbot Coefficients. As we can see all the information contained in the kernel function are transferred in this terms, so in order to characterized the gratins we need to intensify only those terms.

Equation 1.4 can be simplified assuming that the distance between the between the first two grating is similar to the distance between the last two. This approach is indicated as *resonance approximation* and it will be described in Section 1.1.2. It leads to:

$$S(\delta x_s, \eta) = \sum_{l=-\infty}^{+\infty} S_l(\eta)\exp\left[\frac{2\pi i}{d} l\,(\delta x_{tot}(\eta) + \delta x_s)\right] \quad (1.7)$$

where δx_{tot} is the total shift accumulated during the free path evolutions without the third grating shift and η is the difference between L_1 and L_2. As we can see the signal is represented as a sum of oscillating terms in δx_s with a phase proportional to δx_{tot} and amplitude of S_l. This last

terms are directly connected to the interference visibility and are given by:

$$S_l(\eta) = \tilde{D}\left(l\frac{(-\eta)}{L_T}d\right) B^{(1)}_{-Nl}\left(l\frac{(-\eta)}{L_T}\right) B^{(2)}_{(N+1)l}\left(l\frac{NL_1+\eta}{L_T}\right) B^{(3)}_{-l}\left(l\frac{(-\eta)}{L_T}\right) \tag{1.8}$$

Phase Shift

The Eq. 1.7 can be rewritten that highlights the contribution of δx_s and δx_{tot} to the final signal. To do this we will need to consider two properties of the term describe in Eq. 1.8. The first one is $S_l = S_{-l}$; the second one is that S_0 does not dependent on η. In this case $S(\eta, \delta x_s)$ is simplified into:

$$S(\eta, \delta x_s) = S_0(0) + 2\sum_{l=1}^{+\infty} S_l(\eta, \delta x)\cos\left(\frac{l\,2\pi}{d}\,\delta x_s + \delta x_{tot}\right) \tag{1.9}$$

Here it is more clear that the signal detected after the third grating is the average of oscillating therms in δx_s and that the shift accumulated during the interference acts exactly as a phase. While the first one can be set externally, the second one is completely defined by the interferometer.

In general we can divide the phase contribution in two components: one accumulated on the second grating (δx_2) and one on the third one (δx_3). These two shifts are calculated using the firs grating as reference and can be generated by two different reasons: one is the particle beam evolution and a second is the transversal alignment of the gratings. In both cases this contribution will sum up to the total shift as:

$$\delta x_{tot} = -2\delta x_2 + \delta x_3 \tag{1.10}$$

The shift generated by the beam evolution is in particular given by the average transversal trajectory of the particles beam. A clear example of it is effect of misalignment between the gratings and beam. If they are not perfectly orthogonal, the initial traversal velocity of the particle will add a shift respect to the first grating of $\delta x_2 = vT_1$ at the second grating and of $\delta x_3 = v(T_1 + T_2)$. These two contributions will add up as:

$$\delta x_{tot} = v_0\,\frac{(-2T_1 + (T_2 + T_1)}{2} = v_0\,\frac{T_2 - T_1}{2} \tag{1.11}$$

and in particular they will be neglectable if $T_1 \simeq T_2$.

Similar calculation can be done for a more interesting shift, in particular when the particles beam are subject to an external field. If, for

example, the gratings are vertically orientated, the particle will be subjected to the weight force field that will transversely, accelerate them. In this case during the particles will fall [1] of $\delta x_2 = \frac{1}{2} g\, T_1^2$ when they reach the second grating and of $\delta x_3 = \frac{1}{2} g\, (T_1 + T_2)^2$ at the third one. The total shift will be:

$$\delta x_{tot} = g\, \frac{(-2T_1^2 + (T_1 + T_2)^2}{2} = g\, \frac{-T_1^2 + T_2^2 + 2T_1 T_2}{2} \tag{1.12}$$

Unlike the precedent case, this phase contribution will not disappear in case $T_1 \simeq T_2$ and it can be used to estimate g as demonstrated in [12].

The shift generated by the traversal misalignment of the gratings is exactly the same as the one described before. In fact if a grating is shifted of $\delta\tilde{x}_2$ with respect to the first one, it will interact with the matter-wave as the latter is shifted of $\delta x_2 = -\delta\tilde{x}_2$. However in this case it is better not to calculate the shift respect to the first grating but with an external reference. In this way we can manage all three grating separately, so if it is the first one that is shifted we just need to calculate its contribution instead of propagate i8t to the other two gratings. In order to do this we just need to set an external reference $\tilde{x_0}$ and calculate the shift of the grating in function of this. In this way we have that: $\delta\tilde{x}_2 = \delta\tilde{x}_1 + \delta x_2$ and $\delta\tilde{x}_3 = \delta\tilde{x}_1 + \delta x_3$, where the tilde indicates that is calculated from an external reference. In this way the total shift is given by:

$$\delta x_{tot} = -2(\delta\tilde{x}_2 - \delta\tilde{x}_1) + (\delta\tilde{x}_3 - \delta\tilde{x}_1) = \delta\tilde{x}_1 - 2\delta\tilde{x}_2 - \delta\tilde{x}_3 \tag{1.13}$$

Resonance approximation

As anticipated before, Eq. 1.7 and 1.8 are an approximation of the general formulation of the interferometer signal give by Eq. 1.4.

The assumption that connects the general equation to Eq. 1.8 is that, before the first grating, the transversal momentum of the beam has a very wide distribution, in particular that $\sigma_p \gg \frac{h}{d}$. In this case we can assume that $\tilde{D}(s)$ has a sharp distribution and it acts as an exponential suppressor. Based on this idea we can formulate the *Resonance approximation*: the only terms of that can survive Eq 1.4 are those fulfilling the condition $\frac{kL_1 + lL_2}{T_T}\, d < \frac{1}{\sigma_p}$, where we can assume that $\frac{1}{\sigma_p} \ll \frac{d}{h}$.

This approximation can be rewritten assuming that the ration between L_1 and L_2 is closed to an integer: $L_2 = NL_1 + \eta$. In this case we can rewrite $\tilde{D}$ as:

$$\tilde{D}\left(\frac{kL_1 + lL_2}{L_T}\, d\right) \simeq \delta_{k,-lN} \tilde{D}\left(l\, \frac{\eta}{L_T}\, d\right) \tag{1.14}$$

1 In this case we will neglect the initial velocity v_0.

that introduces the selection rule for the order of the Talbot coefficient and reduce the Eq. 1.4 to Eq. 1.7. Even in this approximation, the suppression due to $\widetilde{D}$ it is still present. In particular we can measure it, looking to the visibility in function of the asymmetry parameter η. In this way it is possible to estimate the initial beam divergence and the effect of collimation long the gratings direction. An Example of this suppression is given in Fig 1.3

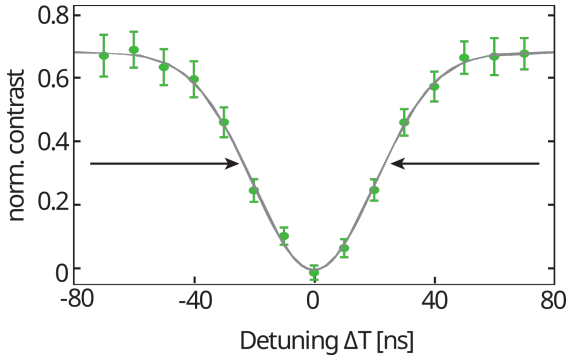

Figure 1.3: In this plot we can see that a small detuning from a Symmetric configuration leads to a suppression of the Visibility. This is exactly the exponential suppressor factor due to $\tilde{D}\left(l\,\frac{\eta}{L_T}\,d\right)$. In particular this is the Visibility contrast of a time domain interferometer, that is explain in Section 1.1.3 and Section 1.2. This figure and a deeply analysis of this measurement can be find in [4].

TIME DOMAIN

A time domain interferometer looks at the interference modulation in time and not in space. To understand better this dualism, it is easier to consider the double slits interference produced by a optical wave and extend it to matter wave case.

Starting from the Fraunhofer diffraction equation, we know that the modulation of the intensity after the slits is given by:

$$I(\vartheta) = \cos^2\left(\frac{\pi d}{\lambda}\sin(\vartheta)\right)\operatorname{sinc}^2\left(\frac{\pi b}{\lambda}\sin(\vartheta)\right)$$

where ϑ is the angle direction of the wave within respect the slits.

In the space domain we fix a longitudinal distance L from the slits and record the intensity in function of transversal position x. In particular we are not interested in the time evolution of the wave but only in its spatial distribution. In fact the previous equation is calculated for a monochromatic continuous wave (CW) which is time invariant. In this

case we can can rewrite the ϑ dependency as $\sin(\vartheta) = \frac{x}{\sqrt{L^2+x^2}}$ and the position of the fringe maximum as:

$$\frac{x_{max}}{\sqrt{L^2 + x_{max}^2}} = n\frac{\lambda}{d}.$$

In the time domain we want to manipulate the fringe in function of the time and in particular we are interested on how the diffraction changes the wave time evolution. We detect therefore both the position and the intensity in function of the time. In this case we cannot use a CW wave because we need a pulsed one with a define group velocity $\mathbf{v}_g$.

For the purpose of this section we do not need to recalculate the modulation of the signal for a pulsed wave but we can assume that inside the package the system will act as a CW with the constrain that the wave needs a time $t = \frac{r}{v_g}$ to reach a distance $r = \sqrt{L^2 + x^2}$ from the slits. In this way we can calculate the trajectory of a maximum that it is given by:

$$\frac{x_{max}}{vt} = n\frac{\lambda}{d} \rightarrow x_{max} = n\frac{\lambda}{d}vt.$$

This dynamics becomes really interesting in the study of matterwave where the group velocity of the wave-function of a particle is directly connected to its wavelength, $\lambda = \frac{hm}{v}$. If we combine this with the previous equation we get:

$$x_{max} = n\frac{\lambda}{d}vt = n\frac{md}{h}t$$

where the group velocity disappears. This means that the transversal position of a maximum is not dependent on the velocity of the particle and it evolution is determinated independently of its previous dynamics.

A similar effect is present in the Talbot-Lau effect. In this case we have to do some assumptions on the gratings: the first one is that we have to be allowed to decide when the particle and the grating can interact, as if we can turn them on and off; the second one is that gratings have to be very wide in order that to the particle can interact long all the longitudinal direction;

In those condition we can assume that if we impose that a particle with momentum p_z interacts with a grating at a time T_i, this will happen at position $L_i = \frac{T_i m}{p_z}$. Using this assumption and the fact that Eq. 1.4 depends on L_i only as a ration with L_T we can rewrite the arguments following this rules:

$$\begin{aligned} L_i &\rightarrow T_i \\ L_T &\rightarrow T_L \end{aligned} \tag{1.15}$$

where T_i is the timing when the i-th grating will interact with the particle and T_T is the Talbot Time given by:

$$T_T = \frac{md^2}{h} \tag{1.16}$$

and the selection rule on L_i will became:

$$T_1 - NT_2 = \tau \simeq 0 \tag{1.17}$$

The selection rule given by the *resonance approximation* leads to same conclusion, where the asymmetry between the spatial distance of the grating will became a asymmetry in between the time distance, in particular se substitution rule is $\eta \rightarrow \tau$.

In this way the interference is not anymore dependent on the velocity of the particle and moreover the idea of wavelength loses a role in the interference measurement and the interference will be function only of the particle mass. This means that we can use sources with wide-velocity distribution and without applying any velocity selector to the beam, as will e discuss in Section 2.4.

OPTICAL GRATINGS

Time domain requires that the gratings interact withe the particles at a precise time. For this reason we cannot use a standard material mask but we need "something" that can appear and disappear in function of an external trigger.

In order to achieve this behavior, we mimic a standard grating using an optical standing waves. Controlling the laser beam that will produce this *optical grating* we can manage to turn it on and off with a time precision given by the pulse source.

In general a material grating acts as a intensity modulator by the elimination of particles in function of their position: the section of the wave that does not cross an aperture will be absorbed from the grating and the local intensity reduced to zero. In case of matter-waves, this modulation can be done by photo-ionization and photo-fragmentation: instead of blocking the particle we can remove from the beam by fragmentation or ionization due to photon absorption. This kind of grating are called *absorptive gratings*.

An other effect generated by the interaction between a particle and a optical grating is a phase modulation. The polarization induced by the optical filed can add a phase to the particle wave-function. This effect is presented only in the middle grating interaction and it contributes to the diffraction of the matter-wave.

The idea behind the generation of a optical grating is that when a laser beam hits perfectly orthogonal a plane mirror, the superposition of the reflected and the incident beams will create a standing wave. This one will have a periodicity of half the wavelength of the original wave and a fixed node on the surface of the mirror. Using a pulsed laser the standing wave will last and act only for the duration of the pulse.

As explained in detail in [13], the interaction between a standing wave and a particle is governed by two parameters: the optical dipole polarizability α, and the absorption cross-section σ_{abs}.

These quantities are representative of the two kind of modulations discussed before: the optical dipole potential will imprint a sinusoidal phase modulation onto center-of-mass state of the particles, where the maximal phase shift Φ_0 is proportional to α. On the other hand, the photon absorption will imprint a modulation amplitude, the probability of a ionization or a fragmentation is proportional to σ and the intensity of the standing wave and like this one is spatially period.

These two modulations are completely described by Talbot coefficient:

$$B_m^{(k)}(\xi) = e^{-n_0^{(k)}/2}\left[\frac{\sin(\pi\xi) - \beta\cos(\pi\xi)}{\sin(\pi\xi) + \beta\cos(\pi\xi)}\right]^{m/2} J_m\left[\operatorname{sgn}\left(\frac{1}{\beta}\sin(\pi\xi) + \cos(\pi\xi)\right)\frac{n_0^{(k)}}{2}\sqrt{\frac{1}{\beta^2}\sin^2(\pi\xi) - \cos^2(\pi\xi)}\right] \tag{1.18}$$

where $J_m(x)$ is the Bessel function of first kind. The interaction between the grating and the particle is given by two parameters present in the equation: $n_0^{(k)}$ that we saw before and and β defined as:

$$\beta = \frac{\lambda\sigma}{8\pi^2\alpha} = \frac{n_0^{(k)}}{2\varphi_0^{(k)}}. \tag{1.19}$$

This last parameter takes into account the phase modulation due to the polarization induce by the optical filed and its contribute is completely marginalized when the argument of the Talbot coefficient is zero. In this case we can rewrite it as:

$$B_m^{(k)}(0) = (-1)^m e^{-n_0^{(k)}/2} I_m\left(\frac{n_0^{(k)}}{2}\right) \tag{1.20}$$

where I_m is the modified Bessel function.

Only the first and the last grating can show this behavior. In particular the third grating acts always like mask, imposing a spatial selection onto

particles. The first one, instead, presets a small phase contribution only when the interferometer is in a asymmetric setup, i.e. $T_1 \neq T_2$, but in general it is also negligible.

The second grating is the only one that shows both amplitude and phase modulation. In this case the presence of the β parameter can shift the time separation T_{max} where we can find the maximum Visibility[2]. Therefore it is not true that $T_{max} = T_T$, but in general the T_T will still maintain an important role in the interference. In fact if we consider the contribution of the diffraction grating:

$$B^{(2)}_{(N+1)l}\left(l\frac{NT_1+\tau}{T_T}\right)$$

we can notice that when $T_1 = T_T$ and we are in a symmetric configuration $\tau = 0$, the argument of the Talbot coefficient is an integer number an in particular we can rewrite as:

$$B^{(2)}_{(N+1)l}(lN) = e^{-n_0^{(k)}/2}\left[\frac{\sin(\pi lN) - \beta\cos(\pi lN)}{\sin(\pi lN) + \beta\cos(\pi lN)}\right]^{m/2} J_m\left[\mathrm{sgn}\left(\frac{1}{\beta}\sin(\pi lN) + \cos(\pi lN)\right)\frac{n_0^{(k)}}{2}\sqrt{\frac{1}{\beta^2}\sin^2(\pi lN) - \cos^2(\pi lN)}\right]$$

that is reduced to:

$$B^{(2)}_{(N+1)l}(lN) = (-1)^{(N+1)l}\, e^{-n_0^{(k)}/2}\, I_{(N+1)l}\left[(-1)^{lN}\,\frac{n_0^{(k)}}{2}\right] \quad (1.21)$$

that is similar to Eq. 1.20. In particular this equation says that if we set the interferometer with a time separation perfectly equal to the particle Talbot Time, the phase modulation is neglected and the middle grating acts as an absorption grating[3].

This model is based on a perfect standing wave and does not consider realistic imperfection such as finite reflectivity and flatness of the mirror and the finite coherent laser to of the standing wave. This correction is explained in [6].

2 This parameter will be discuss in Section 1.2.

3 In particular we have the same results with the limit $\alpha \to 0$.

ESTIMATION OF THE INTERFERENCE CONTRAST

In order to estimate the interference contrast we need to control the interferometer modulation of the signal, that, if we consider the its reformulation wrote in Eq.1.9, is given by:

$$S(\tau) = S_0(0) + 2\sum_{l=1}^{+\infty} S_l(\tau, \delta x)\cos\left(\frac{l\,2\pi}{d}\,\delta x\right)$$

We will consider only the case where $N = 1$, $T = T_T$, so the S_l terms are:

$$S_l(\tau) = \tilde{D}\left(l\frac{\tau}{T_T}d\right) B^{(1)}_{-l}\left(l\frac{\tau}{T_T}\right) B^{(2)}_{2l}\left(l\frac{T_T+\tau}{T_T}\right) B^{(3)}_{-l}(0) \tag{1.22}$$

In most of the cases we can stop to the first order and consider the sinusoidal approximation but a more deeper analysis of that can be find in [7].

If we consider only $l = 1$ the signal after the third grating will be:

$$S(\tau) = S_0(0) + 2S_1(\tau, \delta x)\cos\left(\frac{2\pi}{d}\,\delta x\right)$$

and in this case the easier way to modulate it would be through the shift δx: we just need to record the signal at different position of the third grating δx_s and and estimate the contrast using the standard contrast estimator, the Visibility:

$$\mathcal{V} = \frac{S_{max} - S_{min}}{S_{max} + S_{min}}$$

that will be equal to:

$$\mathcal{V} = 2\left|\frac{S_1}{S_0}\right| \tag{1.23}$$

However this method is not suitable for OTIMA. In fact due to experimental reasons described in Section 2.2.2, we are not able to shift one grating respect the other ones. [4]

Instead of measuring the interference pattern and then estimating the Visibility we can try to measure directly the last one. This concept is

4 However a proof of work of this method was done by Haslinger et al. in [4], but this solution is too time expensive.

based on the ideal setup of the interferometer where all three gratings are perfectly aligned and we can assume $\delta x = 0$.

Starting from Eq. 1.23 we see that in order to estimate the Visibility we need only S_0 and S_1, so in case of OTIMA we just focus on them. The first value can be directly measured exploiting the resonance approximation described in Section 1.1.2: we know that if the argument of $\tilde{D}$, $(l\frac{\tau}{T_T}d)$, is enough different from zero, the S_l therm described in Eq. 1.22 will be suppressed. This can happen only for $l \neq 0$, so assuming a $\tau > 0$, we have that:

$$S(\tau) = S_0(0) + 2\sum_{l=1}^{+\infty} S_l(\tau, \delta x) = S_0$$

In order to achieve this measurement we need to add a time difference between the two grating's time-separation, and for this reason it is called "asymmetric" measurement. The minimum value for τ is imposed by the beam divergence: as explained in Section 1.1.2, the width of $\tilde{D}(x)$ is given by $\frac{h}{\sigma_p}$ so what we need is that $\frac{h}{\sigma_p} < l\frac{\tau}{T_T}d$.

On the other hand, the estimation of S_1 needs a real interference measurement, where $\tau = 0$, called "symmetric" measurement. In this way we will get:

$$S(0) = S_0 + 2S_1$$

and using the information obtained from the other one we can estimate the Visibility:

$$V = \frac{S(0) - S(\delta t)}{S(\delta t)} = \frac{S_0 + 2S_1 - S_0}{S_0} = 2\frac{S_1}{S_0} \tag{1.24}$$

In general we cannot assume $\delta x = 0$, and this can be an issue. In fact if we consider this phase shift we have to rewrite the visibility estimator as:

$$\hat{V} = \frac{S(0) - S(\delta t)}{S(\delta t)} = \frac{S_0 + 2S_1 \cos\left(\frac{2\pi}{d}\delta x\right) - S_0}{S_0} = 2\frac{S_1}{S_0}\cos\left(\frac{2\pi}{d}\delta x\right) \tag{1.25}$$

where we can see that we will always look at an underestimation of V and we can eventually estimate $\hat{V} = 0$ in case the phase $\delta x = \frac{d}{4}$. If this shift is generated from the gratings mismatch, it will be in function of which part of the interferometer mirror we are using, and it is completely random. This is not always a problem since we just need to hit the particles always in the same space point. The real problem is the gravity shift inasmuch it depends on the timing separation of the gratings, so if the gratings condition are fixed it will forbid a periodical range of time configuration of the interferometer.

2

EXPERIMENTAL SETUP

OVERVIEW OF THE EXPERIMENTAL APPARATUS

The OTIMA experimental apparatus can be divided in three main components: source, interferometer, detector respectively. These three components are housed in Vacuum Chambers for different reasons. The first reason is to decrease the presence of residual gasses: this is the first source of background during the signal recording and, it can lead to *collisional decoherence process*[14]. The other main reason is that we use VHU lasers to generate the optical gratings: at this wave-length regime the oxygen component of the air absorbs and reduces the beam length to less that a centimeter.

There are a three separate chambers. The first one is the Source Chamber that is called because hosting only the particles beam source. It is not properly part of OTIMA, since is completely changeable. The detector and part of the interferometer share the Main Chamber, where the optical gratings interact with the molecular beam. This chamber is connected to the Source one by a gate valve that allows to hot-plug the source. In fact this one is the only Very High Vacuum Chamber and hosts the *interferometer mirror* that is the more delicate part of the experiment, so has to be always pumped. The last chamber is the Optical one, where all optics elements are located and control the gratings beams and it is optically connected to the Main chamber by a CaF_2 Windows.

In order to describe the setup we can follow the paths of two main actors that interact in the interferometer: the particles beam that travels from the source to the detector and the light beams that travels from the lasers to the interferometer.

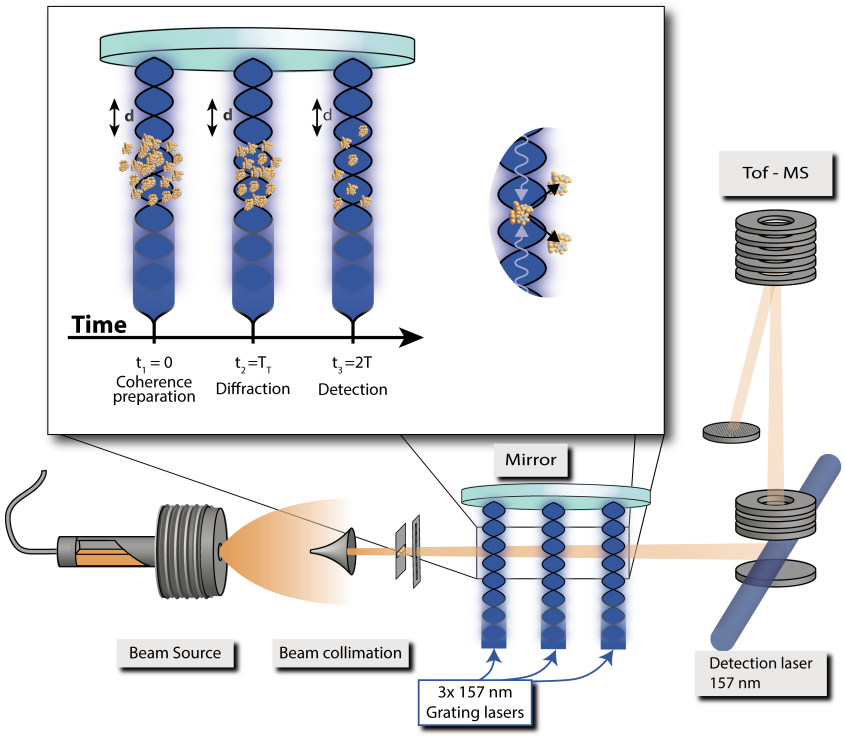

Figure 2.1: This Figure Summarizes the particle path inside the interferometer. From left to right: Particle Source, Collimator, three Optical Grating produce by a single mirror and Detector composed by a ionization laser and a oaToF-MS

THE PARTICLE PATH

The particle path is represented in Fig. 2.1 and it can be schematized as follow:

SOURCE The particles beam is produced by the source hosted in the Source Chamber and enters into the Main Chamber through a gate valve. See Section 2.4, for more details.

COLLIMATION The beam shape is redefined by two slits, one horizontal and one vertical, that are composed by an array of aperture that ranges between 1 mm and 150 µm. We reduce the beam profile for two reasons: the vertical selection ensures that there all the particles will pass inside the grating; the horizontal one allows to control which section of the gratings are used in order to use only a trustable one.

It is important to point out that the reasons of this slits are only geometrical, since we need them only to select spacial extension of the beam and not to reduce the spreading of the transversal momentum distribution.

INTERFERENCE After this preparation the particles beam enters in the interferometer. Here the particle will interact with the gratings, three standing-wave generated by the retro-reflection of laser pulsed beams. The quality of this grating is exponentially reduced within the distance from the *interferometer mirror*, so in order to use the their best section, the particles beam travel closed enough to the mirror that is slightly cut by it.

DETECTION The particles beam travel ended in the detector, that is composed by an ionization laser and a Mass Spectrometer. In this way we can resolve the signal for different masses and measure the last degree of freedom of the interference modulation. See Section 2.3 for more details.

THE LIGHT PATH

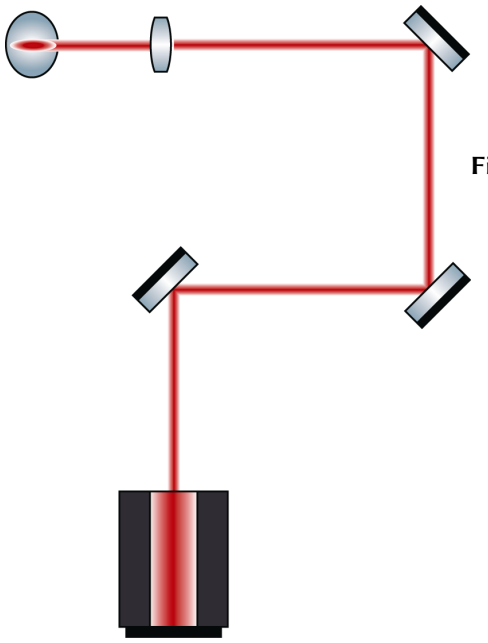

Figure 2.2: This is the basic setup of a laser beam used to generate a optic grating. Starting from the bottom we have the laser source and the first two mirror used for coarse alignment. The last two are remotely controlled by piezo-motors and are dedicate for the fine alignment. The last one is faced orthogonally to the draw.

The three lasers path are almost equal, the only one that has an extra step is the middle one. A general scheme is presented in Figure 2.2 and in particular the single steps are:

LASER SOURCE The three light beams required for the standing-waves are produced from three different F_2 Excimer Laser that are triggered externally. In particular for each sources, the exit windows of the laser cavity are directly connected to the Optic Chamber. For more information see Section 2.2.1

OPTIC CHAMBER The laser beam travels inside the Optics Chamber, that is evacuated up to a residual pressure of 5×10^{-4} mbar and flooded with pure nitrogen in order to prevent damages on the optics. The purge gas can be mixed with oxygen that highly absorbs the laser's wavelength. In this way we can modulate the intensity of the pulses. The middle grating passes thought an mini-chamber hosted inside the Optics one, that is separately flooded in this way its possible to separately modulate its power.

BEAM PROFILE RESHAPE As we will see in Section 2.2.1 the beam profile is rectangular. This shape is manipulated by a cylindrical lens that will shrink the smaller side and it is rotated by a periscope in order to have all the laser profiles parallel to each other and the per particle trajectory.

ALIGNMENT AND STANDING WAVE After this the laser beam is ready to be used in the interferometer, so it is alignment in order to pass through the CaF_2 windows that connect the Optic chamber to the Main one and hits perfectly orthogonal the *interferometer mirror*. The superimposition between the incident beam and the reflected one generates the standing wave that will be used as optical grating. More details about the mirror can be find in Section 2.2.2

INTERFEROMETER

LASER GRATINGS

As anticipated in the previous chapter, the interferometer is composed by three optical standing-waves that act as time domain gratins. In order to generate them, a laser beam is aligned perfectly orthogonal to the interferometer mirror surface. In this way the reflected part can superimpose with the incident one and generate a standing lightwave with a spatial periodicity of $d = \frac{\lambda}{2}$.

From the experimental point of view, the quality of the gratings is described in terms of its visibility, that is limited by the coherent length of the original beam and the reflectivity of the interferometer mirror. Moreover the first and the last grating needs to act as absorption mask, so they need to ionized or fragment the particles. The last request is due to the time domain nature of the interferometer, that requires that the gratings act in a precise times, that means short pulse-width and stable Trigger-to-Emission delay.

For each grating we use a dedicated GAM EX50 F_2, i.e. an excimer laser that works with a gas mixture of Fluorine and nitrogen. This source was chosen for its short wave-length, 157.52 nm, that gives a Talbot Time for mass unit of 15.546 ns u^{-1}. Moreover its energy per photon of 7.92 eV, allows to use a large selection of molecules. The only big disadvantages of this source is the band-width $\Delta\lambda$ =1 pm, that corresponds to a nominal coherent length of 1 cm. This limits the usable range of the gratings to less that half of a centimeter, in particular experimental test reduce the trust reagion to 1 mm.

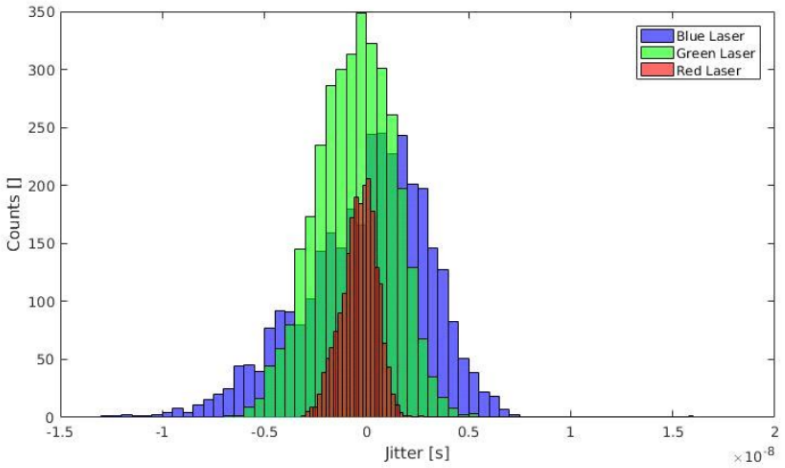

Figure 2.3: Trigger-to-Emission Jitter of three laser: Green is the Preparation , Blue the Diffraction and Red the Detection.

Timing properties of this lasers are enough for a time domain interferometer: we estimate the Trigger-to-Emission (TE) jitter around 5 ns and a FWHM of 3 ns and the nominal duration of the pulse is 10 ns. The gratings stability is increased by real time feedback and post selection of the data. In fact we use two biased GaP photodiodes to record the timing and the intensity of the lasers pulse. In this way we can correct the laser trigger and label every single frame in function of the real time separation of the gratings. In general we se a tolerance of 2 ns of jitter, rejecting about 1 % of the frames.

The beam profile produced by the source has a Gaussian mode with a rectangular shape of 9 mm × 4 mm, with a nominal divergence of 0.8 mrad × 1.4 mrad. The original profile is shrunk using cylindrical lens in order to decrease the thickness to 1 mm. The alignment mirrors are in a periscope configuration that allows us to reorientate the beam profile in order to have the three gratings with the long side parallel to the particles beam.

INTERFEROMETER MIRROR AND GRATINGS

The kernel of this experiment is the interferometer mirror: as studied in [6], its roughness and effective reflectivity are directly responsible of the standing wave quality and its global deformation adds a fixed shift to the interference patter.

The interferometer mirror is a CaF_2 substrate coated dielectricaly in order to have an high reflectivity at 157 nm with a rectangular of shape 7 cm × 4 cm. Its characterization was made by the producer LASEROPTIK GmbH: the reflectivity is higher of 95 % and the usable part is restricted to 5 cm × 3 cm central area where the average roughness is up to 10 nm, as show in Figure 2.4.

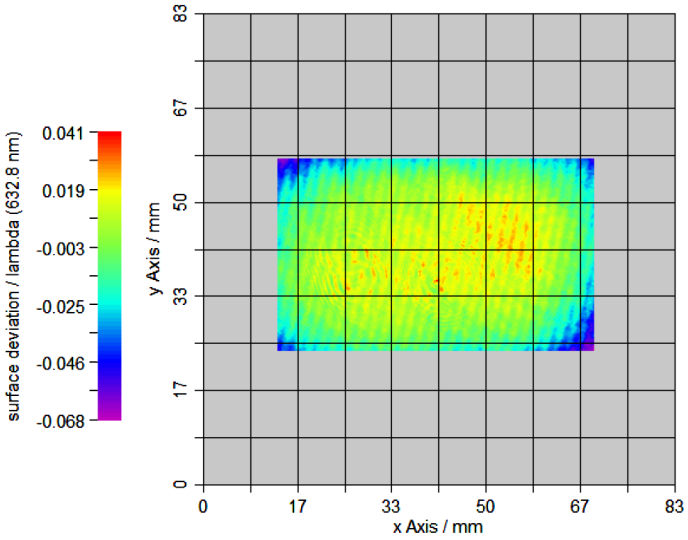

Figure 2.4: Characterization of the interferometer mirror surface done by LASEROPTIK GmbH.

This one is the more delicate element of te interferometer. In fact it is continuously shined with VUV light that locally over coated the surfaces with the beam particle reducing the reflectivity and increasing the roughness of the mirror. This requires to periodically change the hit spots.

GRATING ALIGNMENT

Even if OTIMA is a time-domain interferometer, the spatial alignment of the grating is necessary to obtain a measurable contrast. There are two aspects to keep in mind to align the interferometer: the generation of standing-wave and their position with respect to the particles beam.

If the light beam does not arrive perfectly perpendicular on the mirror, the standing-wave will not have a periodicity of $d = \lambda/2$ but if the incident angle has a deviation of $\delta\vartheta$ from the orthogonality, the slits will be spaced of $\tilde{d} = \frac{\lambda}{2}\frac{1}{\cos(\delta\vartheta)}$, that mismatches the gratings and can blur the interference. [1]

The superposition alignment of the incident and reflected beams is verified looking to the CaF_2 window that divide the Main chamber from the Optic one. This kind of windows are not completely transparent and they absorb between 30 % to 5 % of the light that is remitted in the visible range by a blue fluorescence. This makes it possible to see where the beams cross the window and, overlapping the two spots to impose a maximum $\delta\vartheta$ of $2\,\mathrm{mrad}$.

If part of the particles beam does not pass trough the grating but is anyway detect, the measured signal will have an offset that decreases the contrast. As explained before we reduce the vertical width of the particles beam to less the gratings profile. Moreover to maximize the overlap between we perform a *transition measurement* where we compare the particle signal when the lasers are on and when they are off, and we move the lasers beam in order to minimized their ration. In particular both the alignment are performed simultaneity: we cyclically maximized the particle depletion and realigns the lasers beam orthogonally to the interferometer mirror.

DETECTOR

The detector used to measure particles beam signal is a Time of Flight Mass Spectrometer (ToF-MS), a RFT50 produced by *Kaesdorf*, in Munich, that is orthogonal-accelerated and a reflectron-type. In this kind of ToF-MS, namely oaTof-MS, the particle are ionized by a laser[2] in order to produce charged particles, accelerate them orthogonally with respect to the original beam direction and, after a free-fly path, detect.

This acceleration is given by a Voltage impulse that imprints a initial velocity of $v_0 \propto \sqrt{\frac{m}{z}}$, where m is the mass of the ions and z is its residual charge. After that, the particle freely travel to the detector. In this way it is possible to measure the delay between the detection signal and the acceleration impulse, i.e. the time of free flight of the ions. Due to the fine distance between the enter of the ToF-MS and the detector, this time

1 This mismatch is not always a bad thing: if it is controlled, i.e. in [4], can be used to scan the interference pattern.

2 Florine Excimer Laser,the Coherent EXiStarXS, that has the same wave-length of the grating laser,157 nm but a pulse energy of 2 mJ

interval is proportional to its initial velocity, so to the square root of mass-charge ratio:

$$t_{ToF} = A\sqrt{\frac{m}{z}}.$$

In particular our oaMS-ToF is equipped with a two-field acceleration stage and with an Mamyrin ion mirror, that gives a mass resolution of $\frac{\Delta m}{m} = 5000$. The first reduces the fluctuation contribution due to different starting point of the ions[15][16] while second one corrects the spread energy distribution of the ions[17].

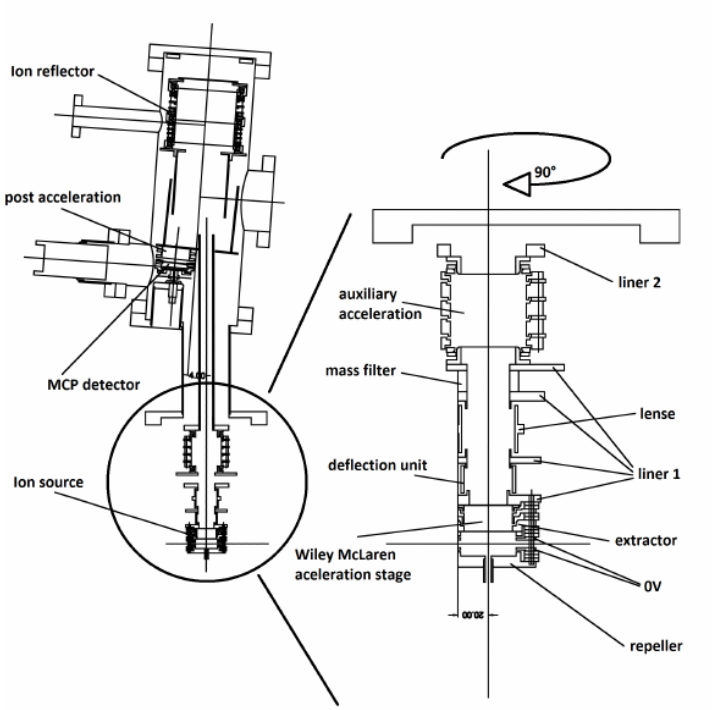

Figure 2.5: Schematic of the RFT50

The ions detector is composed of three Micro-channel plate in Z-stack configuration. This kind of detector is really fast but the quantum efficiency is directly proportional to the ions velocity, that decreases with mass.

PARTICLE BEAM SOURCE

The quality particle source is responsible of two important aspects: one regards the properties of beams as velocity, Trigger-to-Emissions jitter,

signal and pulse size; the other one regards properties of the particles that the source can emit, as stability, mass and absorption cross section.

BEAM PROPERTIES

The perfect beam for OTIMA generates a slow beam with a wide velocity distribution, small pulse length, high and stable signal and low Trigger-to-Emission jitter.

The slow velocity is required due to geometrical constrain: although it is true that OTIMA is velocity independent, we still need to illuminated the particle with three lasers at precise time separation, the Talbot Time. This light beams have a finite size and they cannot be separated too much due to the single mirror setup. This imposes a maximal velocity of:

$$v_{max} = \frac{\delta z}{T_T}$$

where δz is the maximal spatial distance between the gratings.

The wide velocity distribution,together with the low Trigger-to-Emission Jitter, allows to work with different masses, without moving and realigning the grating every time we need to change the Talbot time. Moreover it allows to use always the same part of the gratings, in order to limits contribution of global imperfection of the mirror.

Basically we can use the velocity selection based on the timing of the detector to look at different speed component of the beam. In this way we can fix where particle interact with each grating and use the slower part if we need long Talbot time or the faster one if we need smaller time.

In particular due to the broad velocity distribution, we can change the time between the source shooting and the detection with a neglectable changing of signal. On the other hand, the time stability give us allows to set the precise delay between the emission of the particle and grating *formation*, in particular if we assume to know a first triad of trigger times for the laser (T_i) associated to a detection timing ($T_{det.}$), we can recalculate it for a different Talbot Time using the following relation:

$$\frac{T_i}{T_{det.}} = \frac{T_i'}{T_{det.}'}$$

where T_i are the laser delays in the first set-up and T_i' in the new one.

A wide momentum distribution can also be an issue. If the pulses are too long it can happen that the slower part of a pulse is detected with the faster one of previous one or otherwise. This mixing will increase the background consequently reduces the visibility of the interference.

PARTICLE PROPERTIES

Regarding the molecule, the high absorption cross section for the grating lasers wavelength is a necessary for an absorption grating: as explained before, both the first and the third grating works only if they can deplete particle through absorption of one or more photons.

An other requirement is the thermal stability because emission of photons or fragmentation during the interference process will lead to *thermal decoherence* [18]. For similar reasons a charge particles beam is not suitable for interference due to the easy coupling both between molecule of the same pulse and with external electric noise.

LASER DESORPTION SOURCE

The results presented in this thesis were obtain using a Laser Desorption source. The basic idea behind this is sublimate the particle using a laser pulse. In this way it possible to create a thermal pulsed thermal beam where the heat exchange with is reduce in order to avoid the fragmentation of the particles.

A thermal source is suitable for OTIMA because a fixed *temperature* of the beam give it does not give a velocity distribution but a momentum one and this means that the velocity will inversely proportional to the mass. This fact reduce the constrain caused by the fine dimension of the *interferometer mirror*. On the other hand the thermal launch can excite the internal state and destabilized the particle. This can reduce the visibility by photons emission or fragmentation. The Trigger-to-Emission jitter is directly connected to the pulse laser one, that in general about the order of nanoseconds.

The source mounted in OTIMA is composed by a plate on which the particles are deposited. The layer homogeneity is critical for the beam stability and its thickness for the pulse length. Different techniques were used for the preparation of the samples in function of the different properties of the compounds.

Once it is ready the plate is mounted on inside a Source Chamber at a a distance of 50 cm from the oaMS-ToF. The plate holder is magnetically attached to two orthogonal step motors that can move the plate parallel to its self. In this way we can maintain fixed the laser spot and moving the sample. This allows to use always a fresh part of the particle layer and at the same time keep the source aligned. In fact the beam starting point is completely controlled by the desorption laser one that is focused onto the plate. In order to generate a pulsed laser beam we use a CW source and modulate the beam intensity with a Acousto-Optical Modulator(AOM) that can electronically chop the beam in function of an external trigger.

MEASUREMENT

The measurement protocol adopted by OTIMA is a cyclical acquisition of the Mass Spectrometer signal produced in tow different configurations of the gratings: Interference and Reference. For each one, a particle package is emitted from the source, modulated by the gratings and detected by the MS-ToF and the configurations are repeatedly switched in order to marginalize slow emission drifts of both lasers and particle sources.

In the interference mode we require to the gratings to be symmetric: the delay between the first and the second as to be equal to the delay between the second and the third. In the reference mode we change the middle grating timing in order to have a symmetric configuration of the grating: as explain before, in this way we will record the average signal of the interferometer.

Every single frame recorded from the MCP are labeled using the grating information produce from the photodiodes. During the measurements we record the amplitude and timing of each laser pulse in order to estimate the effective alignment of the grating. In this way we can post-filter the measure in function of the Jitter from the required configuration and the laser power fluctuation.

All the measurements procedure is controlled by M.o.p.s., a custom-made software written by Geyer and deeply described in his PhD thesis [19]. This program manages the timing of all the components, the data acquisition and the on-line pre-processioning of the measurement. At every time a new cycle of acquisition M.o.p.s configure three BNC Model 575 pulse/delay generator that are responsible for all the trigger. For the digital acquisition of the MCP signal is used a ADC card with resolution of 12-bits and sample frequency of 2 GHz, and buffered directly by M.o.p.s.[3].

DATA ANALYSIS

A pre-processing the of the data is necessary due to huge amount of data produce during the experiment. The first selection is done by the jitter and amplitude labels, described in Section 2.2.1. After this, the single frame are digitally filtered and sum up together in function of their labels.

3 DAQ/DigFiltereditizer: ADQ412 4-channel, 12-bit

OLD ANALYSIS METHOD

As explained in Rodewald and Dörre in their thesis [7] [20], in order to estimate the visibility, we record two different set of file: proto-file and zero-file.

The first set (Proto File) is the simple average of every frame produced by the MS-ToF. In this way all the raw pulses, together with the electrical background, will sum up and create the mass spectrum. If we are not in a saturation regime of the MCP detector, we can assume that the amplitude of pulse is proportional to the number of ions that generate it, we have that the integral of our peaks is proportional to the number of particles. That is not guaranteed near or over the saturation region of the MCP, in this case the signal will be an underestimation of our original signal.

The other set (Zeros file) of data is produced by a simple discriminator algorithm, that will put every channel that is over the threshold to $+1$ and $+0$ if that is lower. This converts the ions pulses to a square one and completely cut off all the electronic background and increase the SN ratio. The other advantage of this filter is the possibility of counting the number of ions pulse that contribute to the mass spectrum signal. In fact we have that the integral of a Zero file spectrum will be proportional to the number of ions with a defined time of free fly. This proportional factor is given by the width of the square pulse generated from the discriminator.

Assuming that the detection probability is Poissonian we can estimate the statistical standard deviation of the peaks and, using the Gaussian propagation, estimate the Visibility error. To do that, we focus on the non-events: a Poissonian distribution imposes that the probability to have zero events is $P(0) = e^{-\lambda}$and is $\lambda = \left\langle \frac{K}{N} \right\rangle$, namely the average ration between number of particle K and number of observation N. To estimate the $P(0)$ value we use the ration of number of frames without any ions over total number of frame: $\frac{1-N_{ev.}}{Ntot.}$ and as error to propagate $\sigma_K = \sqrt{K}$.

This method is stable for small counts, High Signal to Noise Ratio (SN) and a linear response from the MCP.

The first request is due to the necessity of having a good estimation of zero-counts, if the ratio of zero-counts is to close to 0 or 1 the probability estimation is not reliable.

If the SN ratio is too low , we have two problems: the first one is the difficultly of discriminating the integration interval; the second one is that the noise will be the major component of the peak integral and its statistical error will not be neglectable.

If the MCP is close to saturation, the amplitude of its signal will not be proportional to the number of particle, but will underestimate it. This systematic error will shift and scale the visibility, as explain in Section 2.6.3.

In the following Section we will present the evolution of this method, the main purpose of this thesis that can be use to in case of small SN and does not require to have a linear signal from the MCP.

NEW ONE

To achieve a trustful estimator of the signal we need to model the entire process leading to the signal.

The first element is the source. In our setup we work with pulsed sources. This type produces a series of packages that contain the same average number of molecular. The first assumption that we do is that our source emits a number of particle with a Poissonian distribution:

$$P(n) = \frac{\lambda^n}{n!} e^{-\lambda}. \tag{2.1}$$

where λ is given from the source configuration and the selection rule applied after.

The second assumption is that if we modulate the beam we are imposing that a particle will survive with probability p. As already describe in Section 1.1.2 the interferometer theory gives us $p = S(\tau)$, the modulation of our original signal. This can be interpreted as the probability that a single particle survive.

If the beam pulse is composed by more that one particle, the probability of getting k of them starting from n trough a modulator is the binomial distribution:

$$P(k|n,p) = \binom{n}{k} p^k (1-p)^{n-k} \tag{2.2}$$

where in the interferometer case $p = S(\tau)$.

The combination of Eq. 2.1 and Eq. 2.2 gives probability of detecting k particle after the interferometer. In particular we are interested in:

$$P(k|\lambda, S(\tau)) = \sum_{n=0}^{+\infty} P(k|S(\tau), n) P(n|\lambda) \tag{2.3}$$

that can be reduce as, :

$$\begin{aligned} P(k|\lambda, p) &= \sum_{n=0}^{+\infty} \binom{n}{k} p^k (1-p)^{n-k} \frac{\lambda^n}{n!} e^{-\lambda} \\ &= \sum_{n=0}^{+\infty} \frac{n!}{(n-k)!k!} p^k (1-p)^{n-k} \frac{\lambda^n}{n!} e^{-\lambda} \\ &= \sum_{n=0}^{+\infty} \frac{1}{(n-k)!k!} p^k (1-p)^{n-k} \lambda^n e^{-\lambda} \end{aligned}$$

using $q = 1 - p$

$$\begin{aligned} &= \frac{p^k \lambda^k}{k!} e^{-\lambda p} \left(\sum_{n=0}^{+\infty} \frac{1}{(n-k)!} q^{n-k} \lambda^{n-k} e^{-\lambda q} \right) \\ &= \frac{(p\lambda)^k}{k!} e^{-\lambda p} \left(\sum_{n=0}^{+\infty} \frac{1}{(n-k)!} \frac{(\lambda q)^{n-k}}{(n-k!} e^{-\lambda q} \right) \end{aligned}$$

where the terms can simplified out using the fact that $n \geqslant k$, so:

$$\left(\sum_{n=0}^{+\infty} \frac{1}{(n-k)!} \frac{(\lambda q)^{n-k}}{(n-k!} e^{-\lambda q} \right) =$$

$$\left(\sum_{n=k}^{+\infty} \frac{1}{(n-k)!} \frac{(\lambda q)^{n-k}}{(n-k!} e^{-\lambda q} \right) =$$

$$\left(\sum_{n'=0}^{+\infty} \frac{1}{(n')!} \frac{(\lambda q)^{n'}}{(n'!} e^{-\lambda q} \right) = 1$$

in function of the we get a Poissonian with a scaled λ:

$$P(k) = \frac{(\lambda p)^k}{k!} e^{-\lambda S(\tau)}.$$

In conclusion the probability distribution of of having k particles is given by:

$$P(k|\lambda, S(\tau)) = \frac{(S(\tau)\,\lambda)^k}{k!} e^{-S(\tau)\,\lambda} \tag{2.4}$$

The other process is the detection that is again Poissonian and the probability to detect k particles is:

$$P(k) = \frac{(\lambda p \mu)^k}{k!} e^{-\lambda p \mu}.$$

where μ is the detection efficiency.

In order to see our particle we use a ToF Mass spectrometer. This detector give us an event every time we detect one or more particles, and, after a calibration, shows us the mass over charge ratio. This is very helpful because give us the possibility to discriminate the last degree of freedom in order to see interference but it does not give us the exact number of particle that passes through the interferometer.

The only information that we have are how many times we detect "something" and how many times we don't. The analysis is based on how many times we don't detect anything. Considering that *don't detect* is a precise number 0 we can focus our analysis on that information.

We know that the probability of having k dark events over n independent measurement is:

$$P(k|n, p_d) = \binom{n}{k} p_d^k (1 - p_d)^{n-k}$$

where p_d is the probability of a single *dark event*, namely a not detected particle:

$$p_d = e^{-\lambda}$$

This can help us to estimate the λ parameter from a measure where we get $\tilde{k}$ dark event over $\tilde{n}$ sample. If we apply the Bayesian theorem we get:

$$P(\lambda|\tilde{k}, \tilde{n}) \propto P(\tilde{k}|\lambda, \tilde{n}) P(p|\tilde{n})$$

where as a prior we can use a uniform distribution:

$$P(p|\tilde{n}) = \begin{cases} 1, & p \in [0, 1] \\ 0, & \text{elsewhere} \end{cases}$$

If renormalized this distribution we get:

$$P(\lambda|\tilde{k}, \tilde{n}) = e^{-\lambda\tilde{k}} (1 - e^{-\lambda})^{\tilde{n}-\tilde{k}} \binom{\tilde{n}}{\tilde{k}} \tag{2.5}$$

.

In order to get the best estimator for the signal we can use the Likehood approach. The basic idea is that the best estimator of λ is the value that maximized its probability and it can be find resolving the equation:

$$\frac{\partial}{\partial\lambda} P(\lambda|\tilde{n}, \tilde{k})|_{\bar{\lambda}} = 0$$

that has a single solution:

$$\bar{\lambda} = -\ln\left(\frac{\tilde{k}}{\tilde{n}}\right) \tag{2.6}$$

An other parameter that is important to estimate is the reliability of this estimator, i.e. its error. In order to estimate it we can expand the probability distribution around its maximum, in particular it is more convenient to expand its logarithm. In this way we can write:

$$\begin{aligned}\ln\left[P(\lambda|\tilde{n},\tilde{k})\right] &= \ln\left[P(\lambda|\tilde{n},\tilde{k})\right] + \\ (\lambda-\bar{\lambda})\frac{\partial}{\partial\lambda}\ln\left[P(\lambda|\tilde{n},\tilde{k})\right]\Big|_{\bar{\lambda}} &+ \\ (\lambda-\bar{\lambda})^2\frac{\partial^2}{\partial\lambda^2}\ln\left[P(\lambda|\tilde{n},\tilde{k})\right]\Big|_{\bar{\lambda}} &+ O((\lambda-\bar{\lambda})^3\end{aligned} \tag{2.7}$$

where the linear terms is null since the maximum of $P(\lambda|\tilde{n},\tilde{k})$ is a maximum of its logarithm. This expansion can be rewritten as:

$$P(\lambda|\tilde{n},\tilde{k}) = A\exp\left[(\lambda-\bar{\lambda})^2\frac{\partial^2}{\partial\lambda^2}\ln\left[P(\lambda|\tilde{n},\tilde{k})\right]\Big|_{\bar{\lambda}}\right]$$

i.e. in the neighborhood of a maximum, the probability distribution of λ can be approximated as a Gaussian distribution with mean $\bar{\lambda}$ and variance:

$$\sigma^2_{\bar{\lambda}} = -\frac{\partial^2}{\partial\lambda^2}\ln\left[P(\lambda,\tilde{n},\tilde{k})\right]\Big|_{\bar{\lambda}}$$

Using this approach we can calculate the λ estimator error :

$$\bar{\lambda} = -\log\left(\frac{\tilde{k}}{\tilde{n}}\right) \tag{2.8a}$$

$$\sigma^2_{\bar{\lambda}} = \frac{\tilde{n}-\tilde{k}}{\tilde{n}\,\tilde{k}} \tag{2.8b}$$

In this way we can estimate λ that as explained before is a combination of three factor: source, interferometer and detector:

$$\lambda = \mu_{src}\,\mu_{det.}\,S \tag{2.9}$$

where S is the signal given from the interferometer theory. The first two terms are not a problem in the visibility estimation because they are only scalar factor that self-simplify out of the equation:

$$V_N = \frac{\mu_{src}\,\mu_{det.}\,S_{int} - \mu_{src}\,\mu_{det.}\,S_{ref}}{\mu_{src}\,\mu_{det.}\,S_{ref}}$$

We can do the same calculation with λ and the result is the same.

The real problem of this analysis is to get a trustful estimation of $\bar{k}$ and $\bar{n}$.

Defined $\bar{x}$ as the true valor and $\tilde{x}$ the estimate one, we have that:

$$\tilde{\lambda} - \bar{\lambda} = -\log\left(\frac{n-\tilde{k}}{n}\right) - \left(-\log\left(\frac{n-\bar{k}}{n}\right)\right) = -\log\left(\frac{n-\tilde{k}}{n-\bar{k}}\right)$$

so if we consider that $\tilde{k} = \bar{k} + \epsilon$ we can rewrite:

$$\tilde{\lambda} = \bar{\lambda} - \log\left(1 - \frac{\epsilon}{n-\bar{k}}\right). \tag{2.10}$$

In this case we have an overestimation of our signal, so exactly the opposite of what happens with the method described before this thesis.

OVERESTIMATION OR UNDERESTIMATION

It is important to understand how an overestimation or an underestimation of the signal can affect the visibility. In order to have a general presentation we can define some variable as follow: our real signal will be $\bar{\lambda}$ and the estimate one $\tilde{\lambda} = \text{bar}\lambda + \xi$ where ξ is the overestimation ($\xi \geqslant 0$) or the underestimation $\xi \leqslant 0$.

This polarization will also affect the Visibility estimation:

$$\tilde{V}_N = \frac{\tilde{\lambda}_{mit-\tilde{\lambda}_{asi}}}{\tilde{\lambda}_{asi}} = \frac{\bar{\lambda}_{mit} + \xi_{mit} - \bar{\lambda}_{asi} - \xi_{asi}}{\bar{\lambda}_{asi} + \xi_{asi}}$$

that can be rewritten as:

$$\tilde{V}_N = \bar{V}_N\left(\frac{\bar{\lambda}_{asi}}{\bar{\lambda}_{asi} + \xi_{asi}}\right) + \frac{\xi_{mit} - \xi_{asi}}{\bar{\lambda}_{asi} + \xi_{asi}} \tag{2.11}$$

Our Visibility estimator is then a rescaling and translation of the real value.

In case of an overestimation of the signal, ξ is always positive and we have that the scaling factor will reduce the visibility. We cannot say much about the shift terms, without making any assumptions. The most plausible one is that, assuming ξ proportional to λ, we have the relation: if $\lambda_i > \lambda_j$ then $\xi_i > \xi_j$. This will lead to say that the sign of the shift term is concordant with the Visibility one and it will increase its module.

In conclusion we have that the overestimation of λ will produce a systematic error of which we cannot estimate a prior orientation.

This problem can be a limit using a live-processing of the signal. If for every peak we know when multiple events happen and how many pulses they have, we can renormalized the single discriminate pulse.

SIGNAL OVER BACKGROUND RATIO STABILITY

An other interesting study on those methods is to see what happens when we have a background due to residual ions near the detector. This scenario is quite common and easily modeled. In particular following the same arguments used before, we can assume that the background has a Poissonian time distribution and we can estimate the average signal as λ_{bg}. In this case we have that the sum of two stochastic processes follows again a Poissonian distribution, with average $\lambda_S = \lambda_{\bar{S}} + \lambda_{bg}$, where the bar indicates the true value. In this case the Visibility estimator is:

$$\tilde{V_N} = \frac{\lambda_{mit} - \lambda_{mit,\,bg}}{\lambda_{asi} - \lambda_{asi,\,bg}} \tag{2.12}$$

and the error is estimate by linear propagation:

$$\sigma_{V_N} = (V_N + 1)\sqrt{\frac{\sigma^2_{mit} + \sigma^2_{mit,\,bg}}{(\lambda_{mit} - \lambda_{mit,\,bg})^2} + \frac{\sigma^2_{asi} + \sigma^2_{asi,\,bg}}{(\lambda_{asi} - \lambda_{asi,\,bg})^2}} \tag{2.13}$$

In this scenario it is really important to identify the background because a wrong estimation of λ_{bg} will lead to a bias on the Visibility, i.e. see interference where it is not or do not see it where it is.

Even if the identification of the Background is trustful, the quality of the signals can reduce the estimator efficiency. In order to study this problem, part of the present work was focused to propose a new method to estimate the visibility. Here is presented a simulation of Visibility measurements in function of the Ration between the Reference Signal and the Background (SBR). This parameter is chosen to representative of the signal quality because it can be estimated by the original source signal and from the Transmission measurement of the lasers. In practices the background will not be affected by the lasers grating and the Reference signal is just the residual one after the gratings laser depletion.

This simulation is based on the concept that both the Reference and the Interference signals are generated as sum of two stochastic variables, one for the real signal($\bar{S}$) and one for the background (Bg), and it is filtered by a discriminator. Basically for each frame four different signal are obtain: Reference(S_{asi}), Interference(S_{mit}) and two estimations of the Background (Bg_{asi} and Bg_{mit}).

The first two are generated as sum of two independent Poissonian distribution $\bar{S_i}$ and $\bar{Bg_i}$ with mean $\bar{\lambda}_i$ and $\bar{lambda}_{Bg_i}$ and the simulated signal is obtained from:

$$S_i = \begin{cases} 1 & \text{if} \quad \bar{S} + Bg > 0 \\ 0 & \text{if} \quad \text{otherwise} \end{cases}$$

and the last two are simply generated as:

$$Bg_i = \begin{cases} 1 & \text{if} \quad \bar{Bg}_i > 0 \\ 0 & \text{if} \quad \text{otherwise} \end{cases}$$

The signals generated in this way are summed over N frames and after that are used to estimate the Visibility $\tilde{V}$.

This simulation need only two real parameters: λ_{Bg} and the number of frames N. All the other parameters can be estimated in function of the expected Visibility V_{ex} and the SBR. In particular:

$$\lambda_{asi} = (SBR - 1)\lambda_{Bg}\lambda_{mit} \quad = (V_{ex} + 1)\lambda_{asi}$$

In order to understand the added value of the proposed estimator,it is presented the analysis of both model, the old one that uses the raw integration and the new one where is applied the Bayesian approach. For both of them I will study the trueness and precision, this two parameter represent the two important aspects of an estimator. The trueness is a description of the difference between the estimator's expected value $\hat{V}$ and the true one $\bar{V}$ and it is represented by the bias:

$$\text{Bias}[\hat{V}] = \frac{\langle V \rangle - \bar{V}}{\bar{V}}.$$

On the other hand, the precision represents the variability of the estimator due to stochastic nature of the process and it is described by the RMS of the estimation value, renormalized on the estimation of the Visibility:

$$\text{RMS}_{\text{rn.}} = \frac{\text{RMS}_V}{\bar{V}}$$

where the RMS is estimate over multiple realization of the simulation. This parameter can also be interpreted as true value of the variability estimator, so it used to calculate its Bias:

$$\text{Bias}[\hat{\sigma}_V] = \frac{\tilde{\sigma}_V - \text{RMS}}{\text{RMS}}.$$

where we estimate use the median to as representative of the σ_V distribution and RMS as true value.

Based on this idea two sets of plot are generated from the signal condition of the AgSF2 measurement that it will be discussed in the Section 3.1.1. In particular I used the lower bound of background's value for the peak of 6.8 ku and number of frame, used in for the interference estimation.

The simulation is done for different values of Visibility from −25 to 25 and SBR from 1.5 to 50, plus a zoom in the range from 1.5 to 10 and

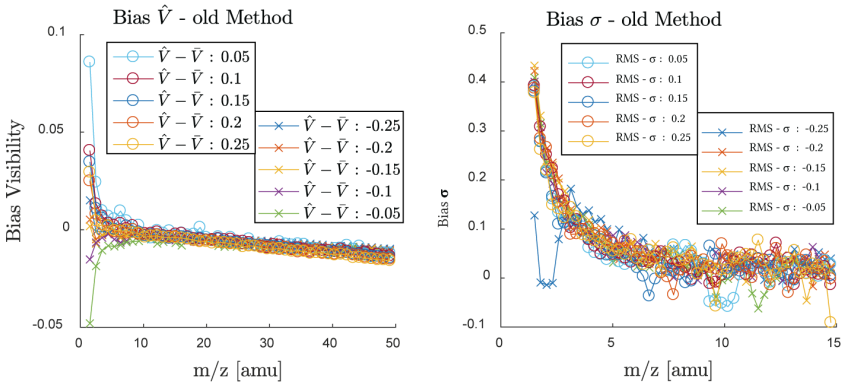

(a) *Bias Visibility estimator.* **(b)** *Bias σ estimator.*

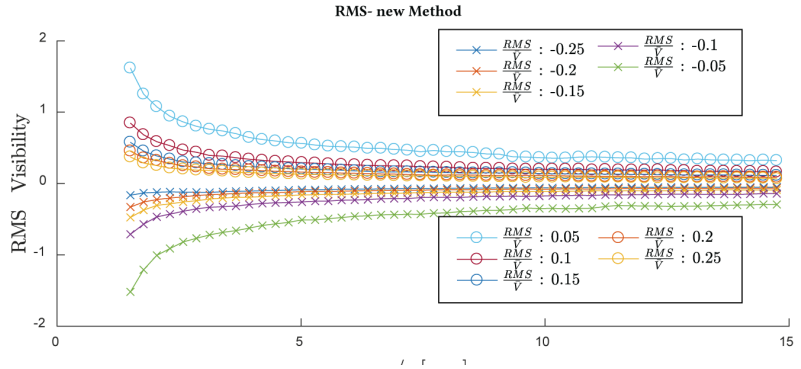

(c) *RMS Visibility estimator.*

Figure 2.6: In this plots we can see the accuracy parameters of the new estimator.

for each combination of this two parameter I simulated 1000 experiment. In this way I mange to estimate both bias and the standard deviation of the Visibility estimation.

In Figure 2.6 the accuracy parameters of the new estimator are plotted. As we can see all three parameters used for the quality analysis show a stable behavior for high SBR: both the visibility and σ estimators have constant bias respectively of the order of 0.1 % and between -1 % and 15 %. The last one is due to an application of the Taylor expansion without consider the correlation between the parameters. This approach is safe when the error contribution are small and there is not strong non linear dependence from the variable. The last request is not fulfilled by the logarithm relation between the frequency of events and the λ parameters. Although in the same region the estimator precision is also stable but it shows a strong dependence from the Visibility but in the stable regime it is always less that 50 %.

These informations allow us to consider the estimator trustable for SBR more that 4 and moreover they suggest about the maximal significant digits that we can use: the visibility bias give us a maximum of 3 digits directly on $\hat{V}$ while the σ one indicates a indirect limits by giving only 1 digits on the error.

In the case the SBR is less that 10 the estimators start to not work properly: the Visibility and σ bias start to increase and the variance reach the same magnitude of the expectation value. In this region the estimator is not completely trustable.

The old method is reported in Figure 2.7 for comparison, where we can see that we have the same general behaviors but with some difference that make the new one more reliable. In this case the Visibility estimator presents a linear bias that increase with the SBR, so better the signal more the estimator goes away from the real value. Furthermore the error estimator trends to underestimate the RMS but the bias is smaller that the new method's one, due to a more linear dependency form the parameters.

In conclusion the new method developed in this thesis is more reliable of the old one because even if there is a stronger bias on the error estimation it trends to be an overestimation and so it is more safe. Moreover the linear bias off the old Visibility estimator does not allow to be used for high SBR.

However the new algorithm can be still improved applying the Bayesian framework directly on the Visibility parameter, in order to avoid all the approximation made during the calculation.

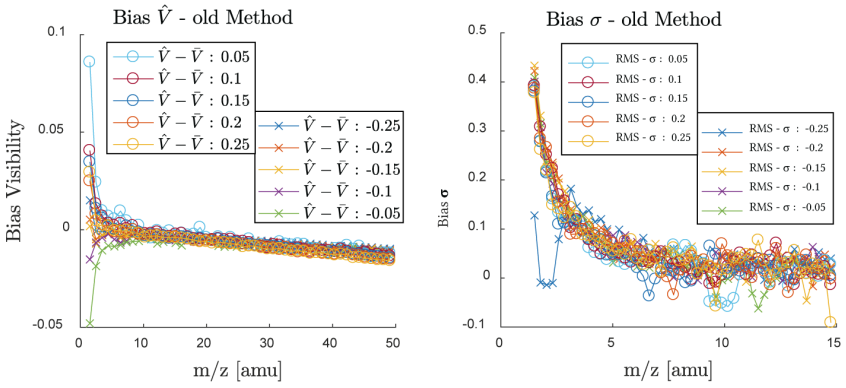

(a) *Bias Visibility estimator.*

(b) *Bias σ estimator.*

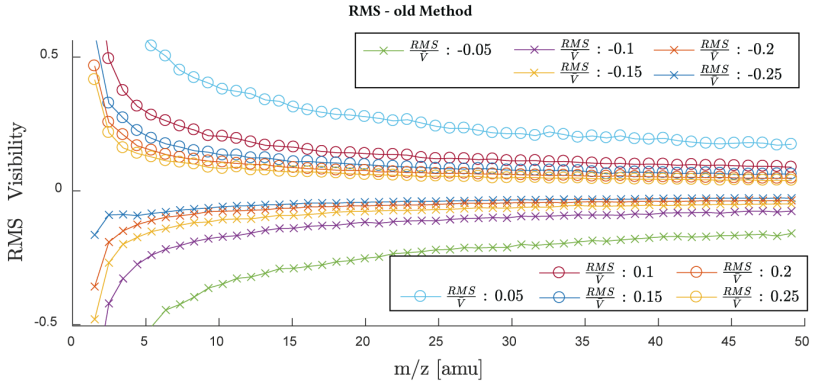

(c) *RMS Visibility estimator.*

Figure 2.7: In this plots we can10 see the accuracy parameters of the old estimator.

3

AGSF2 CLUSTERS INTERFERENCE MEASUREMENT

The main goal of OTIMA was to measure interference with heavy particles, in order to go beyond the actual mass record of 10 123 u [8]. The main problem of working with high mass particles was the velocity constrain discussed in Section 2.4: if we want to measure interference with masses of 10 ku we need a maximum velocity about 160 m s^{-1}. in order to achieve such results, we used a thermal beam generated by a laser desorption source, that we have previously describe in Section 2.4. The molecule choice is more complicated and limited by the states of art of molecules beam technology. Even if this kind of source is widely used in molecular beam experiments, producing a neutral beam of stable and heavy particle is still an experimental challenge.

An option to overcome this problem and that showed great results in Matter-wave interferometery was the exploitation of tailored nanoparticles. The idea was to design and synthesize molecules with the requested properties, such as volatility, mass and absorption cross section for the grating's wavelength.

The first approach to this kind of molecule was done in collaboration with the group of Professor Marcel Major from the chemistry department at the University of Basel. The nanoparticles was based on tetraphenylporphyrin (TPP) core functionalized by perfluoroalkyl chain in order to decrease intermolecular interaction and their increase volatilization ability[21]. In particular, after a pretest of this molecule[22], OTIMA showed interference with: TPP(614 u), $TPPF_{84}$(2815 u) and TPPF(20 — x + 17x) (only at 5560 u)[7].

In this thesis we exploited a second set of molecule based on silver nano-particles capped by perfluoroalkyl chains. In particular, we used the F13-AgNP2 library described in [23]. The first mass spectrum were recorded with a linear ToF-MS, it showed a mass distribution from 5000 u to 17 000 u where six libraries of has been identified by the different ra-

tion between number of ligands and silver atoms Furthermore they were thermally launched without fragmentation and with slow average velocity and high signal.

EXPERIMENTAL APPROACH TO THE INTERFERENCE WITH AGSF2

AGSF2 PREPARATION

After the characterization discussed in [23], the AgSF2 particles were tested in the real interferometer. Unfortunately, due to the different setup, we were not able to reproduce all their results in OTIMA. In particular the signal detected of the heavy libraries was significantly lower compared with the expected one and the spectrum presented an envelop in the region of interest. A spectrum recorded with the OTIMA Tof-MS is showed in Figure 3.1.

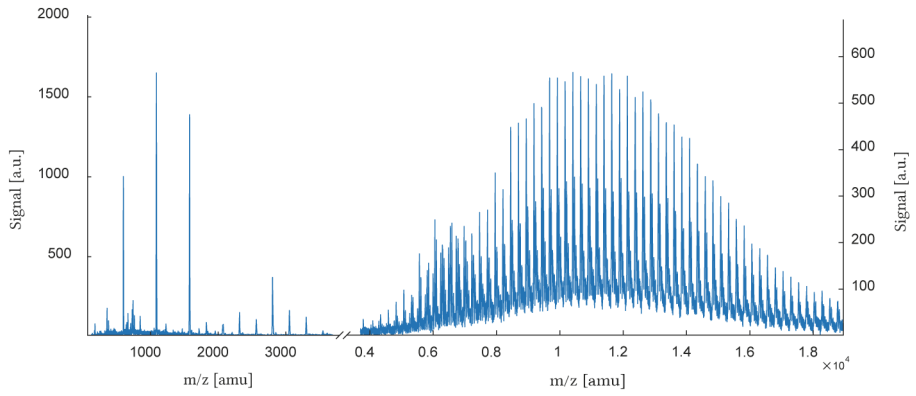

Figure 3.1: Here we can see that the AgSF2 Spectrum recorded from OTIMA. This plot is divide in two in order to discriminated two different particles family. The left one is the range between 600 u and 4000 u, namely the small masses. The right one is between between 4 ku and 16 ku and we will refer to them as high masses. It is important to highlight that the two spectrum has different scale of Signal intensity.

The main differences between the two experiments relied on the position of the source. During the characterization, the plate coated with the nano-particles was put under and very close to the entrance of the ToF-MS, approximately 5 cm , on the other hand in OTIMA the plate had to be in the separated chamber and was 50 cm away from the ToF entrance. This difference is relevant if we consider that the signal of a pulsed source is inversely proportional to d^3.

As explained before, the Visibility estimation is unreliable for SBR lower that 15 and indeed the first goal of our work with the AgSF2 particles was to increase the signal qualities as stability and SBR. We approached this problem from two different point of view: we first worked on the detection in particular we optimized the ions detection in the MS-ToF and signal post-analysis in order to increase the detection efficiency and the SBR. After that we worked on the source in order to increase the signal intensity produced. As we will see the improvements expected were not completely achieved and consequently the final approach was not successfull.

Detection optimization

The first attempt on the detection optimization was the data preselection. We used a discriminator filter in order eliminate the two main noise components: the electrical interference and the backgrounds ions. The first one had an average amplitude of 20 time less that the signal of the particles, so a simple lower threshold discriminator was enough to eliminate it.

The background ions were more complicated to remove since their signal was similar to the beam particles' one. The only difference was that the peaks generated by the residual gas were not time correlated with their masses, so they spread all over the spectrum.

In order to limit the ions background noise we used both upper and lower thresholds that allowed us to resolve the high mass libraries. An example of this filtering is showed in Figure 3.2. As we can see the High mass library was completely hiden from the background noise and only using this technique we were able to distinguish it. This was not enough, the SBR Ration is about 20, that is still not enough for an interference measurement. In fact if we consider the typical configuration of the gratings, we have that each one would transmit only 30 % of the original Signal, so at the end of the interferometer it will be reduced to about 3 % and in our case the SNR will almost one.

The second attempt to increase the SNR was to replace the detector (MCPs). In Figure 3.4 is reported a comparison between the MCPs change, in particular is presented a scatter plot between the pulse time and its amplitude. As we can see the old MCPs (3.4a) was not able to amplify the signal of the High mass library and in particular all the peaks higher that 600 were in fact due to noise. This explains why we were not able to see the masses peaks without put an upper limit to the amplitude discriminator. On the other hand the new MCPs increased the signal so much that it started to saturate the ADC card and more important it separated itself from the electrical noise. In this way the AgSF2 spectrum

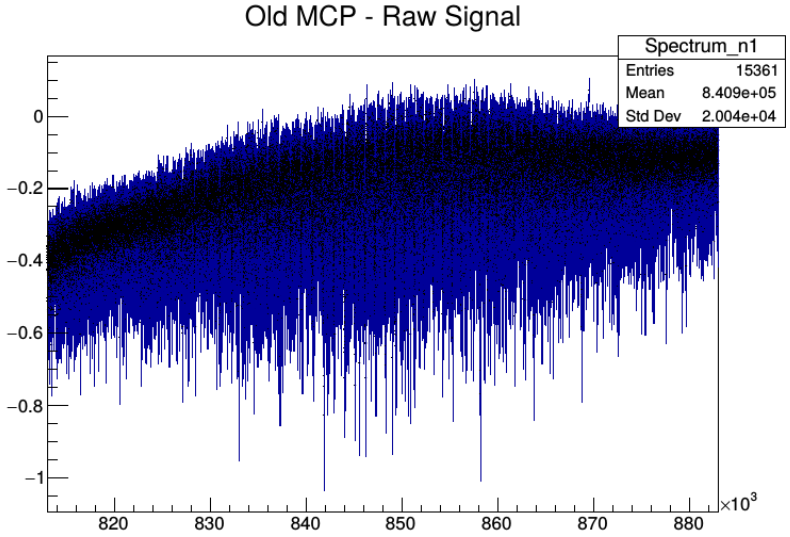

(a) Raw Signal

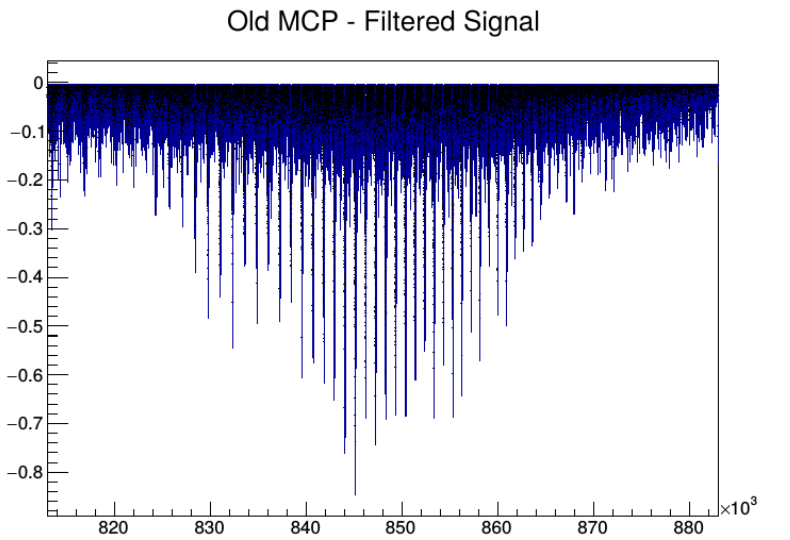

(b) Filtered Signal

Figure 3.2: In this plot is reported the raw signal form the the MCP and its filtered counterpart. In this case we put to 0 every point that was outside the range −45 to −600 and keep the raw value otherwise.

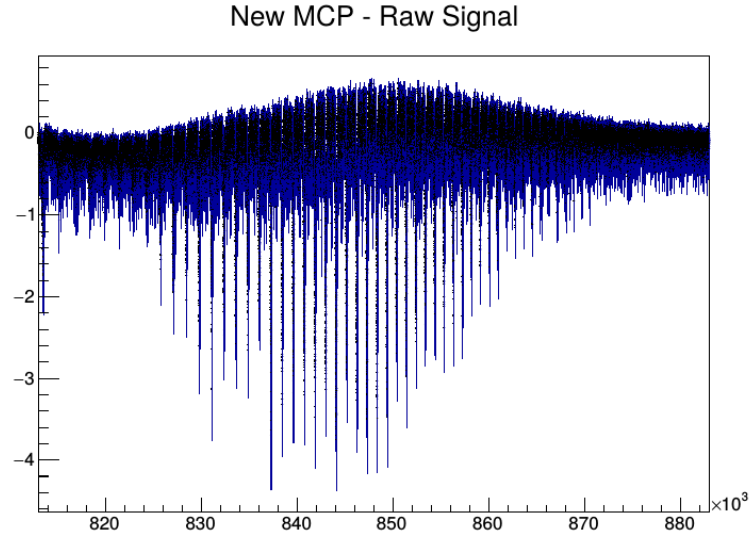

(a) Raw Signal

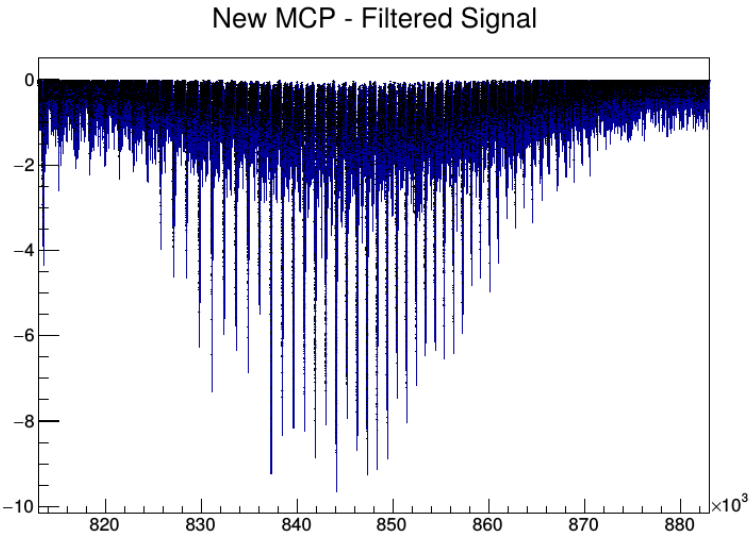

(b) Filtered Signal

Figure 3.3: In this plot is reported the raw signal form the the new MCP and its filtered counterpart. In this case we did not set an upper limit, so the filter keeps the raw value for every point that is lower that −40.

showed up in the raw averaged signal and the SNR increased of a factor 6, as we can see in Figure 3.3.

Source optimization

After working on the detection part, we focused on the source and in particular we tried different approaches on the samples preparations. Considering that a thermal velocity of $150\,\mathrm{m\,s^{-1}}$ for particle of 10 ku required a temperature of about 13 kK it was unlikely that the evaporation was only due to the F13-AgNP2 heating. A possible mechanism is that the remaining ligands not attached to the cluster core acted like a matrix and helped the particle evaporation. So we assumed that signal could depend on the preparation of the particle layer. Starting from this idea we tried different recipes with the goal of achieve higher signal and SBR.

The AgSF2 samples were delivered from Basel in powder and in order to have an homogeneously layer on the plate, we needed to suspend these in a volatile solvent. The original recipe was based on mixing the part of the sample with THF and sonication bath. In the first trials we used different solvents as Toluene and HBF but there was no upgrade on the signal produced. After that we tried to add a matrix of TPP to facilitate the sublimation but we did not see any improvement either.

Another problem occurred was in the composition of the powder delivered from Basel. During the experiment period, we received different batches of the nanoparticles and their composition was not always the same: some samples did not contain the high mass libraries. Even if these batches were not usable for the interference measurements, they gave some more information about the signal. The only thing that we detected in the same range where we expected the high mass library peak, was the envelop. This was always present when we work on AgS2 spectrum using OTIMA, but before this measurement was identified as convolution of the large number of mass peaks. After this measurement we could not assume that as only justification for the envelop and we start to explore different hypothesis. The most reasonable one was fragmentation inside the ToF line: if some nanoparticles fragmented during the free path, the correlations between mass and Time of Fly will blur leading to a visible reduction of the resolution. In order to verify this hypothesis, further analysis should be need but these were not possible due to limited amount of samples. In any case this fact cannot be ignored and it will be taken in consideration for the background estimation.

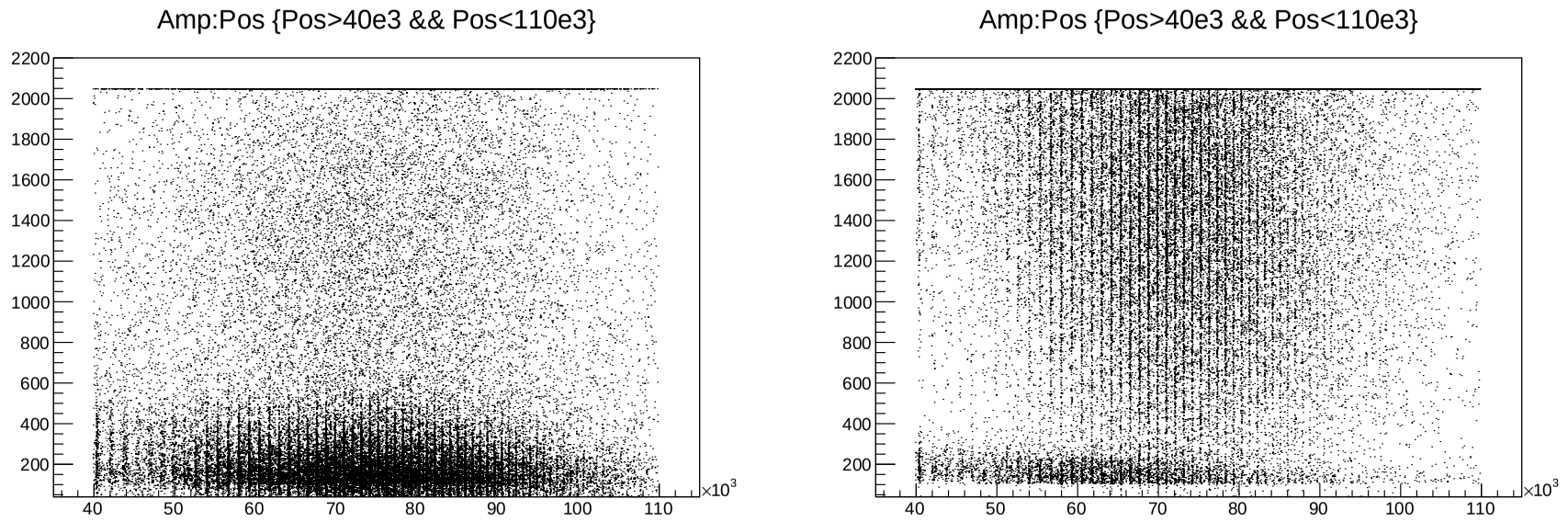

(a) Old MCP

(b) New MCP

Figure 3.4: Those plots represent the time distribution of the peaks. For every single frame we search for peak and record time position and amplitude. The peak search was done, using the algorithm presented in [24] and implemented in the TSpectrum library.

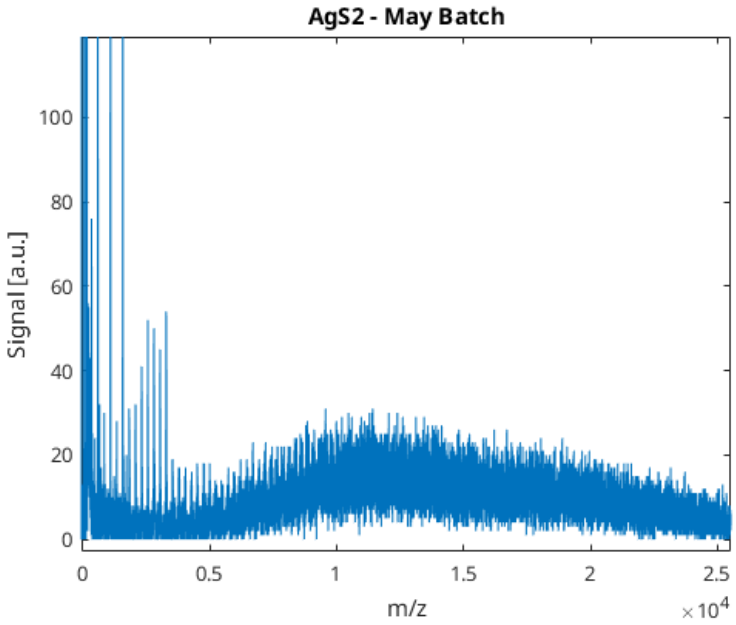

Figure 3.5: Here we can see that the mass region where we were interested showed no peaks, but the envelop remains.

INTERFEROMETER PREPARATION

The main problem of $AgSF_2$ was the limited quantity of samples available. So in order to achieve interference with this nanoparticles and without misspend samples, we used TPP as test particle. This molecule was suitable for alignments and calibrations of the interferometer since it showed a stable behavior.

This particles were deposited by evaporation: a small quantity of TPP powder was heat-up in dedicate a vacuum chamber and the produced vapor was collected by a glass plate placed over the oven. In this way the layer produced was homogeneous and gave a stable and high signal. In this way it was possible to perform real time transmission measurement for the gratings alignment. Moreover the small mass 614.74 u gave a Talbot Time of 9.49 µs that allowed us to test different lasers timing in order to scan a broad range of configuration and to test how much visibility we would expect.

INTERFERENCE MEASUREMENTS

We initially tested the low mass elements of the library, up to 3000 u. These peaks correspond to small $AgSF_2$ particles and they had an high SBR, 6.5~9.2. Moreover this class of molecules was always present in all the batches and it was not affected from the "envelop". We set the

interferometer with a Talbot Time of 84 µs and we recorded the visibility measurement for the masses: 610 u, 1100 u and 1590 u. The interference is showed in Figure 3.6, together with the TPP pretest.

The tree peaks showed different Visibility values in accord with the mass modulation of interference signal. In particular we have 0.24(2) of 610 u; 0.23(2) for 1100 u and 0.06(2) for 1590 u.

After that we started to work on the high mass particle. In this case we had the different problem presented before, envelop and low SBR, of which the more important was the last one that we did not manage to increase.

The only solution that we were able to try was to increase the statistics in order to limit the low SBR effects. So we first checked the interference with TPP for a time separation of 103.9 µs and, after that, we recorded for three days collection slightly more that 1 200 000 frames for each mode. The final mass spectrum is showed in Figure 3.7 together with the mass modulation of the Visibility, calculated assuming $\beta = 1$ and getting $tn_0^{(1)}$ from depletion measurements. As we can see we expected a contrast between 6.2 ku and 8.6 ku.

As anticipated, in this region was presented a envelop that made complicate to identify the background. This is a critical topic because an overestimation of the background will lead to an overestimation of Visibility and vice versa. As we said before we were not able to investigate this envelop and in order to be sure, in this work two background identification will be presented. The first one was based on the signal recorded after 20 ku. The second one is based on the region slightly on the left of each mass peak. The first one is a lower limit that considers only free ions and the possible thermal discharge of the MCPs; the other one is an upper limit that consider as background the envelop. Using these two the definitions of background we evaluated every main peaks in the range from 4 ku to 16 ku.

In Figure 3.8 it is reported, the Visibility estimation using as definition of the background the latest part of the spectrum. The minimum SBR estimate is 5.0so in theory we could trust the estimation for each peak considered. On the other side we don't have contrast in region where we expected (grey box), the Visibility estimated for the these peaks is between $-0.01(3)$ and $-0.06(3)$. Moreover, at higher masses we get value of between 0.15 and -0.15 that are not compatible with zero when the theoretical contrast of this region is zero. In this region the peaks quality is lower that what the SBR calculation indicate, as showed in Figure 3.11, this indication that using only a global background leads is not trustable.

In the second case, the estimation of the background was based on the envelop. In this case we were overestimating the the background inasmuch this envelop was also formed by the convolution of the multitude

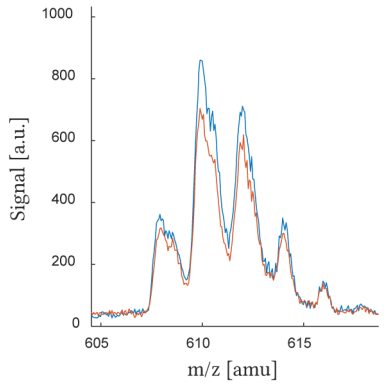

(a) Mass 610 u, SBR 6.5, Visibility 0.23(2)

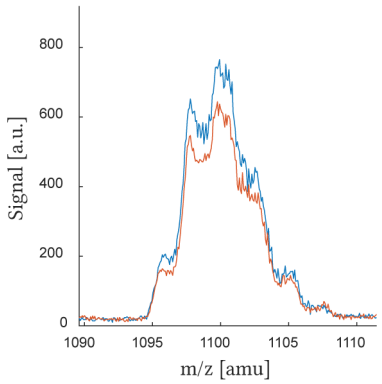

(b) Mass 1100 u, SBR 6.6, Visibility 0.24(2).

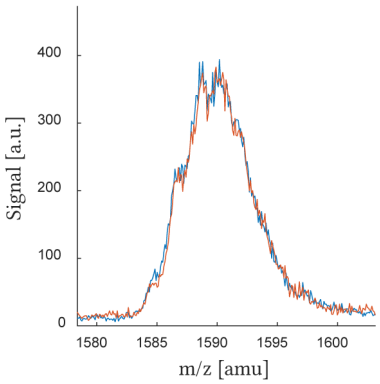

(c) Mass 1590 u, SBR 9.2, Visibility 0.06(2).

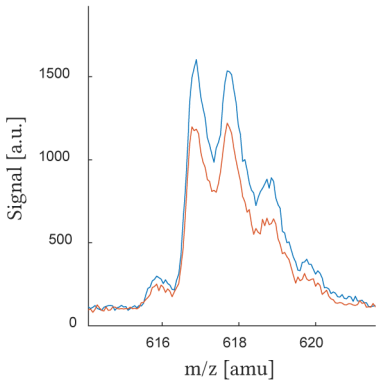

(d) Mass 617 u, SBR 6.5, Visibility 0.27(2).

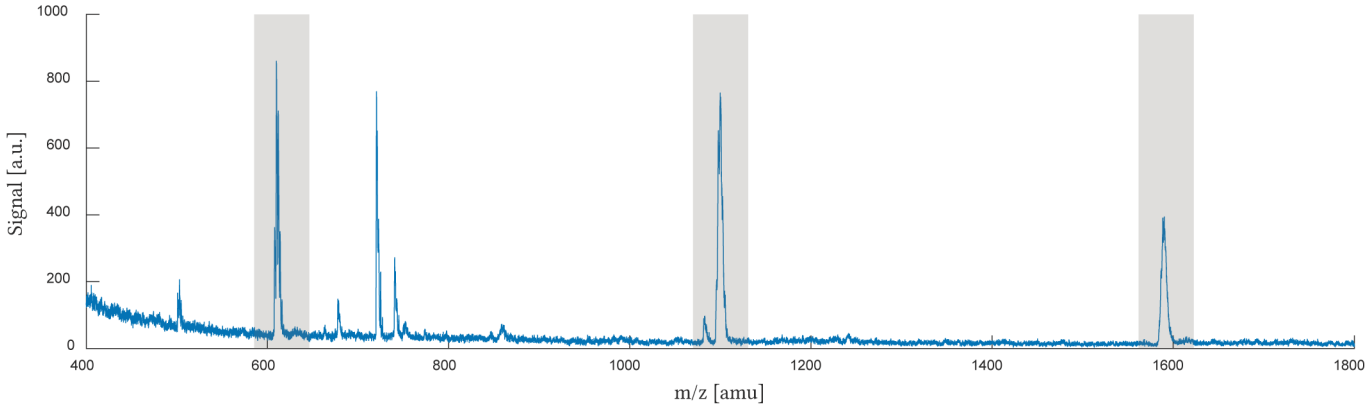

(e)

Figure 3.6: Those plot represent the interference of the small masses component of the AgS2 library. On top and from right to left we have 610 u, 1100 u and 1590 u. The bottom plot represent the mass modulation of the visibility.

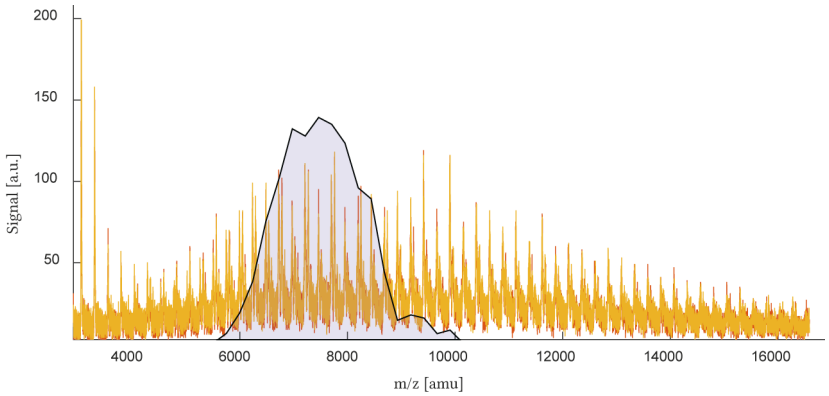

Figure 3.7: Here is reported the AgSF2 spectrum collected for the interference measurement together with the mass modulation of the visibility.

of peaks presented in this region. Moreover depletion measurement suggested that this envelop was part of the beam particle that pass trough the interferometer inasmuch its signal was reduce by the lasers. In conclusion we cannot say that this envelop was completely background, but we can approximately assume that it does not contribute to the interference and we can consider it as upper limit for the background. In particular the chose of the *left* side is due to the presence of smaller peaks on the right of the main one. The results of this evaluation are reported in Figure 3.9. In this case the SBR varied by 1.54 and 3.05 for the peaks from 4 ku to 16 ku and in the range where we expect contrast the minimum raised to 2.00. This situation is the complete opposite of the precedent one, here the SBR is too low to completely trust the estimator, but the values obtained are more in accord with the theory. In particular the visibility estimation for the high masses shows a unstable behavior only for peaks with SBR less that 2.0 (circle marks), where the simulation presented in Section 2.7 showed strong bias. Ont The other

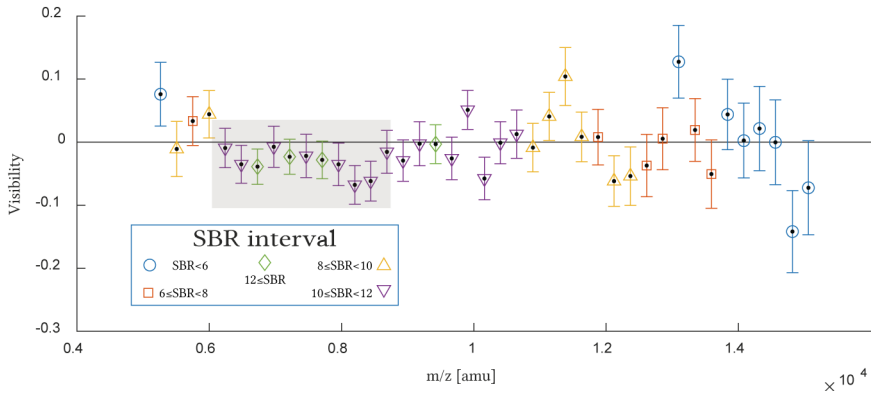

Figure 3.8: In this plot is reported the visibility estimate using the global background. The highlight area indicate the mass peak where we were expecting interference.

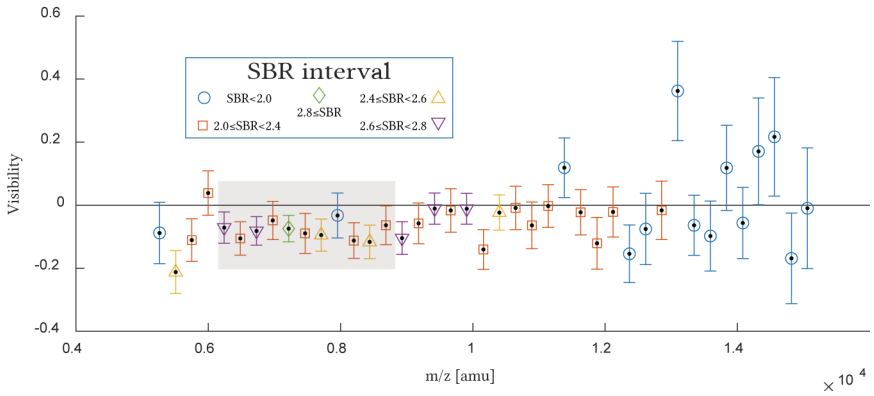

Figure 3.9: In this plot is reported the visibility estimate using the local background given by the envelop. The highlight area indicate the mass peak where we were expecting interference.

hand the visibility estimated in the range where we expected contrast is between $-0.01(5)$ and $-0.12(5)$ that is but it is too low to can assert if this is real interference or just a consequence of the overestimation of the background.

In conclusion we were not able to trust the Visibility estimator with both the global and local identification of the background. In particular the analysis done with the global showed high instability and suggests that the envelop contributes as background during an interference measurement. On the other hand the local identification of the background was partially inconclusive due to the low signal accumulated.

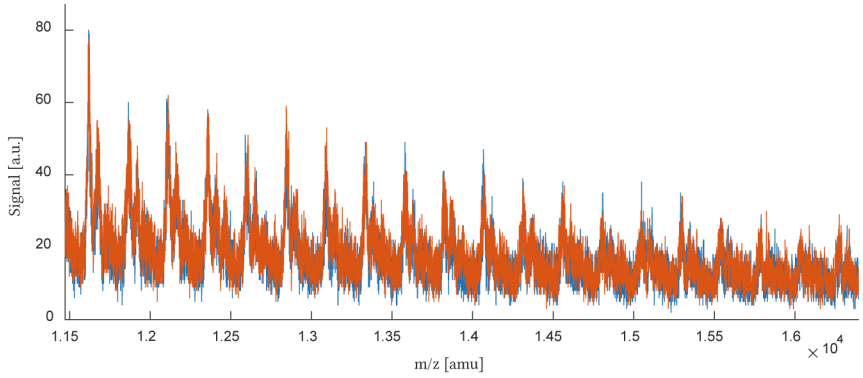

Figure 3.10: In this plot is reported the AgSF2 mass peaks in the region where we expected interference.

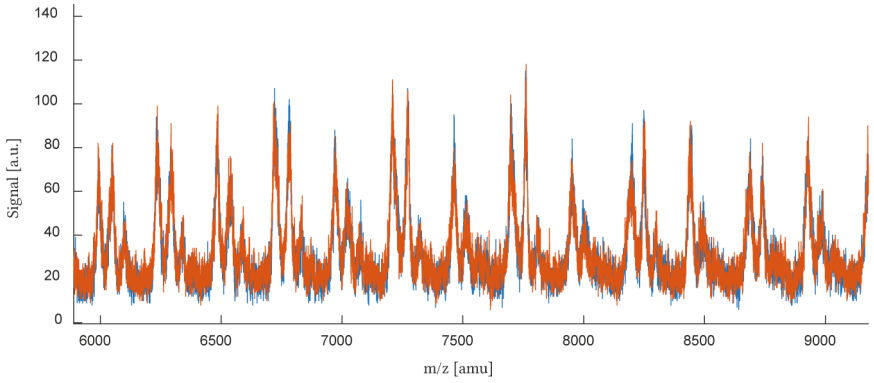

Figure 3.11: In this plot is reported the AgSF2 mass peaks in the region where the Visibility estimation based on the global background gave untranslatable value.

4

CONCLUSION

In this Thesis we presented the a new method to estimate the Visibility of the interference pattern and the results of the last measurement with tailored nanoparticles.

The new estimator is based on a Bayesian approach and it shows to be more robust to systematic errors that the old one. In particular this estimator is based on the analysis and modeling of the signal measured in both two interference mode and after using these value to calculate the Visibility parameter. This approach is still incomplete and can be improved working directly on the Visibility and modeling its statistical behavior. In this way it will be possible to include the correlation between the two signal used to measure and get a better estimation of the Visibility errors.

Moreover, the study about the overestimation of the signal suggests some upgrade into the frames pre-processing. The discriminator filter presented in Section 2.6.1 is not completely suitable for the new estimator. In fact it can lead to a wrong estimation of pulses number for a mass peak and and consequently a wrong estimation of the signal. There are two main reasons for these problems: first the square pulse generate from it does not have stable properties since it area is proportional to the original pulse width at the threshold level; second if two pulse are recorded in a single frame they will be counted as two event instead of one[1].

Starting from these observation we can upgrade the discriminator in order to avoid both the problems. For the first one we just need to fix the width of the logical pulses generated. In this way the signal generate from the filter will be directly proportional to the number of ions detected without extra calibration. On the counter side just fixing the wide of the pulse can lead to a reduction of the time resolution due to time-walking effect. An optimal solution is given by a Constant Fraction

1 When we presented the estimator algorithm, we assumed that the integral of a filtered mass peak was proportional to the number of frames with one or more pulse associated to that mass.

Discriminator that identifies the pulse time independently from its amplitude. This Discriminator can by implemented both analogically(CFD) and digitally(dCFD) but in general the first one has better time resolution. The basic idea of this discriminator is to split the incoming signal in three component. The first two are used for the time analysis: one is delayed of a time t_d and amplified of a factor a. After that it is feed to a comparator together with the other one. The third component is use to select the amplitude of the incoming signal: it is directly feed to a comparator that will generate a logic pulse if the amplitude of the pulse fulfill the threshold. The output from both the comparator are fed in AND gate and will generate the final signal.

For the second problem we can rethink part of the real-time preprocessing as follow. The goal is to know how many frames have recorded at least one ions associated to a precise mass. In order to achieve this we need to identify the integration interval associated to a mass peak. After that we can use this interval to identify each pulse that associated to the mass peaks and increase a counter if there is any. In this way we will integrate the mass peak frame by frame and we can avoid the double counting problem.

Regarding the last results in the high mass interference, the $AgSF_2$ first tests showed promising results but due to the low signal and the limited sample of these nanoparticles we were not able to measure contrast for the range between 4 kuand16 ku. On the other side, we develop experimental procedures that partially overcome the problem and that will be helpful in the new line of research. In the next generation of experiments OTIMA will work on Matter-Wave enhanced Spectroscopy where the sensibility of the interference to external perturbation will used to assist recoil spectroscopy of a large varieties of molecule. In this case the focus of the experiment will be on the particle properties, the only degrees of freedom usable to calibrate OTIMA are the the detector and the interferometer. In this case the experiences with a low signal source will be useful to optimize the particle detection without changing the source condition.

BIBLIOGRAPHY

[1] Angelo Bassi, Kinjalk Lochan, Seema Satin, Tejinder P. Singh, and Hendrik Ulbricht. Models of wave-function collapse, underlying theories, and experimental tests. *Reviews of Modern Physics*, 85(2): 471–527, 2013. ISSN 00346861. doi: 10.1103/RevModPhys.85.471. (Cited on page 1.)

[2] Jonas Rodewald, Philipp Haslinger, Nadine Dörre, Benjamin A. Stickler, Armin Shayeghi, Klaus Hornberger, and Markus Arndt. New avenues for matter-wave-enhanced spectroscopy. *Applied Physics B*, 123(1):3, jan 2017. ISSN 0946-2171. doi: 10.1007/s00340-016-6573-y. URL http://link.springer.com/10.1007/s00340-016-6573-y. (Cited on page 1.)

[3] U. Even. The Even-Lavie valve as a source for high intensity supersonic beam. *EPJ Techniques and Instrumentation*, 2(1):17, dec 2015. ISSN 2195-7045. doi: 10.1140/epjti/s40485-015-0027-5. URL http://epjtechniquesandinstrumentation.springeropen.com/articles/10.1140/epjti/s40485-015-0027-5. (Cited on page 1.)

[4] Philipp Haslinger, Nadine Dörre, Philipp Geyer, Jonas Rodewald, Stefan Nimmrichter, and Markus Arndt. A universal matter-wave interferometer with optical ionization gratings in the time domain. *Nature Physics*, 9(3):144–148, 2013. ISSN 17452473. doi: 10.1038/nphys2542. URL http://dx.doi.org/10.1038/nphys2542. (Cited on pages 2, 11, 16, and 25.)

[5] Nadine Dörre, Jonas Rodewald, Philipp Geyer, Bernd Von Issendorff, Philipp Haslinger, and Markus Arndt. Photofragmentation beam splitters for matter-wave interferometry. *Physical Review Letters*, 113(23):233001, dec 2014. ISSN 10797114. doi: 10.1103/PhysRevLett.113.233001. URL https://link.aps.org/doi/10.1103/PhysRevLett.113.233001. (Cited on page 2.)

[6] Nadine Dörre, Philipp Haslinger, Jonas Rodewald, Philipp Geyer, and Markus Arndt. Refined model for Talbot–Lau matter-wave optics with pulsed photodepletion gratings. *Journal of the Optical Society of America B*, 32(1):114, 2015. ISSN 0740-3224. doi: 10.1364/JOSAB.32.000114. URL https://www.osapublishing.

org/abstract.cfm?URI=josab-32-1-114. (Cited on pages 2, 15, and 24.)

[7] Jonas Rodewald. *Experiments with a pulsed Talbot Lau matter-wave interferometer*. PhD thesis, 2016. (Cited on pages 2, 16, 30, and 41.)

[8] Sandra Eibenberger, Stefan Gerlich, Markus Arndt, Marcel Mayor, and Jens Tüxen. Matter–wave interference of particles selected from a molecular library with masses exceeding 10 000 amu. *Physical Chemistry Chemical Physics*, 15(35):14696, 2013. ISSN 1463-9076. doi: 10.1039/c3cp51500a. URL http://pubs.rsc.org/en/Content/ArticleLanding/2013/CP/c3cp51500a{#}!divAbstracthttp://xlink.rsc.org/?DOI=c3cp51500a. (Cited on pages 2, 3, and 41.)

[9] O. Carnal and Jo Mlynek. Youngs double-slit experiment with atoms: A simple atom interferometer. *Physical Review Letters*, 66 (21):2689–2692, 1991. ISSN 00319007. doi: 10.1103/PhysRevLett.66.2689. (Cited on page 3.)

[10] Kai Walter. *Coherence and Decoherence in High-mass Matter-wave Interferometry*. PhD thesis, 2016. (Cited on page 3.)

[11] Stefan Nimmrichter and Klaus Hornberger. Theory of near-field matter-wave interference beyond the eikonal approximation. *Physical Review A - Atomic, Molecular, and Optical Physics*, 78(2):023612, aug 2008. ISSN 10502947. doi: 10.1103/PhysRevA.78.023612. URL https://link.aps.org/doi/10.1103/PhysRevA.78.023612. (Cited on page 7.)

[12] Jonas Rodewald, Nadine Dörre, Andrea Grimaldi, Philipp Geyer, Lukas Felix, Marcel Mayor, Armin Shayeghi, and Markus Arndt. Isotope-selective high-order interferometry with large organic molecules in free fall. *New Journal of Physics*, 20(3):033016, mar 2018. ISSN 1367-2630. doi: 10.1088/1367-2630/aaade2. URL http://stacks.iop.org/1367-2630/20/i=3/a=033016?key=crossref.4f1234ab8ddf8245cfaaa116ddca4655. (Cited on page 10.)

[13] Stefan Nimmrichter, Philipp Haslinger, Klaus Hornberger, and Markus Arndt. Concept of an ionizing time-domain matter-wave interferometer. *New Journal of Physics*, 13, 2011. ISSN 13672630. doi: 10.1088/1367-2630/13/7/075002. (Cited on page 14.)

[14] Klaus Hornberger, Stefan Uttenthaler, Björn Brezger, Lucia Hackermüller, Markus Arndt, and Anton Zeilinger. Collisional Decoherence Observed in Matter Wave Interferometry. *Physical Review Letters*, 90(16):160401, apr 2003. ISSN 0031-9007. doi: 10.

1103/PhysRevLett.90.160401. URL https://link.aps.org/doi/10.1103/PhysRevLett.90.160401. (Cited on page 19.)

[15] W C Wiley and I. H. McLaren. Time-of-flight mass spectrometer with improved resolution. *Review of Scientific Instruments*, 26(12): 1150–1157, 1955. ISSN 00346748. doi: 10.1063/1.1715212. (Cited on page 26.)

[16] Imma Ferrer and E. Michael Thurman. *Liquid Chromatography Time-of-Flight Mass Spectrometry*. 2009. ISBN 9780470137970. (Cited on page 26.)

[17] B A Mamyrin, V I Karataev, D V Shmikk, and V A Zagulin. The mass-reflectron, a new nonmagnetic time-of-flight mass spectrometer with high resolution. *Sov. Phys. - JETP*, 37(1):45–48, 1973. ISSN 1063-7761. (Cited on page 26.)

[18] Lucia Hackermüller, Klaus Hornberger, Björn Brezger, Anton Zellinger, and Markus Arndt. Decoherence of matter waves by thermal emission of radiation. *Nature*, 427(6976):711–714, 2004. ISSN 00280836. doi: 10.1038/nature02276. (Cited on page 28.)

[19] Philipp Geyer. *Matter-wave interferometry with complex nanoparticles*. PhD thesis, 2015. (Cited on page 29.)

[20] Nadine Dörre. *Time-domain matter-wave interferometry with clusters and large molecules*. PhD thesis, 2016. (Cited on page 30.)

[21] Philipp Schmid, Frederik Stöhr, Markus Arndt, Jens Tüxen, and Marcel Mayor. Single-photon ionization of organic molecules beyond 10 kDa. *Journal of the American Society for Mass Spectrometry*, 24(4):602–608, 2013. ISSN 10440305. doi: 10.1007/s13361-012-0551-3. (Cited on page 41.)

[22] Uğur Sezer, Philipp Schmid, Lukas Felix, Marcel Mayor, and Markus Arndt. Stability of high-mass molecular libraries: the role of the oligoporphyrin core. *Journal of Mass Spectrometry*, 50(1):235–239, jan 2015. ISSN 10765174. doi: 10.1002/jms.3526. URL http://doi.wiley.com/10.1002/jms.3526. (Cited on page 41.)

[23] A. Gallego, Uğur Sezer, Markus Arndt, and Marcel Mayor. Long-pulse laser launch and ionization of tailored large neutral silver nanoparticles with atomic mass assignment. *Nanoscale*, 9(26):9175–9180, 2017. ISSN 2040-3364. doi: 10.1039/C7NR03297H. URL http://xlink.rsc.org/?DOI=C7NR03297H. (Cited on pages 41 and 42.)

[24] M.A. Mariscotti. A method for automatic identification of peaks in the presence of background and its application to spectrum analysis. *Nuclear Instruments and Methods*, 50(2):309–320, may 1967. ISSN 0029554X. doi: 10.1016/0029-554X(67)90058-4. URL http://linkinghub.elsevier.com/retrieve/https://doi.orgpii/0029554X67900584. (Cited on page 47.)